ANL-79-102

353
2/19/80

DR 698

ANL-79-102

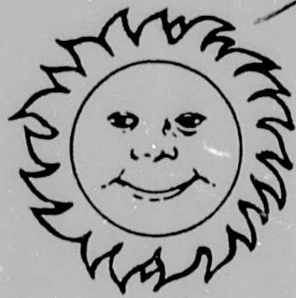

DESIGN OF A SYSTEM USING CPC COLLECTORS TO COLLECT SOLAR ENERGY AND TO PRODUCE INDUSTRIAL PROCESS STEAM

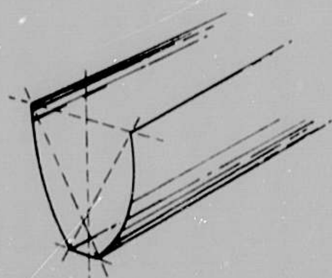

by

C. K. Hsieh

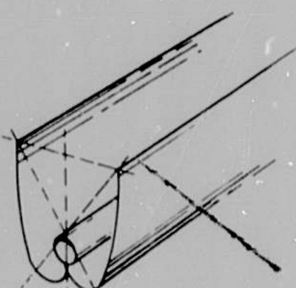

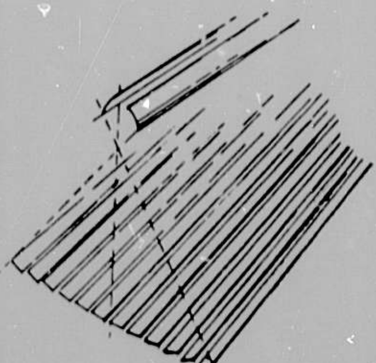

MASTER

U of C-AUA-USDOE

ARGONNE NATIONAL LABORATORY, ARGONNE, ILLINOIS
Prepared for the Office of Solar Applications
Assistant Secretary for Conservation and Solar Energy
U. S. Department of Energy
under Contract W-31-109-Eng-38

Distribution Category:
Heating and Cooling—Research
and Development (UC-59c)

ANL-79-102

ARGONNE NATIONAL LABORATORY
9700 South Cass Avenue
Argonne, Illinois 60439

DESIGN OF A SYSTEM USING CPC COLLECTORS TO COLLECT SOLAR ENERGY AND TO PRODUCE INDUSTRIAL PROCESS STEAM

by

C. K. Hsieh*

Solar Energy Group

August 1979

*Department of Mechanical Engineering,
University of Florida, Gainesville

TABLE OF CONTENTS

LIST OF FIGURES

LIST OF TABLES

NOMENCLATURE

English Alphabet:

A	Area
CR	Concentration ratio
C	Specific heat
D	Hydraulic diameter
d	Diameter
e	Heat exchanger effectiveness
F	Frictional coefficients, $F' = U_o/U_L$, F_R [Equation (31)] F_x [Equation (46)], F_A [Equation (44)]
f	Drag coefficient
G	$\dot{m}_c/A_a$
g	Gap, acceleration
H	Solar flux
h	Convective coefficient, enthalpy
i	Incident angle on cover
j	Incident angle on receiver envelope
K	Permeability
k	Incident angle on receiver jacket, thermal conductivity
L	Length of trough, length of heat pipe and its sections
M	Mach number
$\dot{m}$	Mass flow rate
N	Number
Nu	Nusselt number
n	No. of reflections
p	Gap, pressure
Q	Heat flow
q	Heat flux
R	Thermal resistance, gas constant
r	Radius
S'	Equation (27)
s	Tensile stress
T	Temperature
t	Thickness
U	Loss coefficient, overall heat transfer coefficient, conductance
V	Wind speed, flow velocity
W	Half width of aperture, shaft work
x	Quality of steam

Greek Alphabet:

α	Absorptance
γ	Specific heats ratio
ϵ	Emittance
η	Efficiency
θ	Acceptance half-angle
μ	Viscosity
Σ	Surface tension
ρ	Reflectance, density
σ	Stefan-Boltzmann Constant
τ	Transmittance, shear stress
ϕ	Wick porosity
ψ	Tilt angle

NOMENCLATURE

Subscripts:

A	Enclosure absorption
a	Collector cover, heat exchanger inner radius, annulus, heat pipe adiabatic section
b	Beam component, ambient, boiler loop
c	Convection, collector circulating fluid, capillary, condenser
d	Diffuse component
e	Receiver envelope, heat pipe evaporator section, effective conductivity
f	Fluid, mean fluid temperature, back plate
g	Receiver wall
h	Hydraulic radius
i	Inside radius, inlet section, inside surface
IR	Infrared
L	Loss coefficient from receiver surface to ambient
l	Liquid
m	Mirror, mesh wire
n	Nucleus Radius
O	Overall loss coefficient
o	Outside radius, optical efficiency, stagnation state, exit
p	Heat pipe, pipe wall, constant pressure condition
ph	Preheater
R	Heat recovery factor
r	Receiver
s	Sky, static pressure
t	Total
u	Useful heat gain, ultimate tensile strength
v	Vapor or vapor core
w	Wick
x	Heat Exchanger
-	Mean value

DESIGN OF A SYSTEM USING CPC COLLECTORS TO COLLECT
SOLAR ENERGY AND TO PRODUCE INDUSTRIAL PROCESS STEAM

by

C. K. Hsieh

ABSTRACT

A system has been designed to use CPC collectors to collect solar energy and to generate steam for industrial process heat purposes. The system is divided into two loops with the collectors in the collector loop to operate a preheater and the collectors in the boiler loop to heat water to elevated pressures and temperatures. A flash boiler is used to throttle the heated water to steam. Two types of CPC collectors are chosen. In the collector loop the CPC collectors are fitted with concentric tube receivers. In the boiler loop the collectors employ heat pipes to transmit heat. This design is able to alleviate the scaling and plumbing problems. A fragile receiver tube can also be employed without rupture difficulties.

The thermal processes in the collectors were analyzed using a computer modeling. The results were also used to develop a thermodynamic analysis of the total system. Calculations show that the design is technically feasible. The CPC collector is shown to have an efficiency that is very weakly dependent on its operating temperatures, which makes the collector particularly attractive in high temperature applications.

I. INTRODUCTION

The use of compound parabolic concentrator (CPC) to collect solar energy has received much attention in recent years. The CPC is able to offer a concentration ratio that is the highest possible given the acceptance angle of the device [1]. Because the CPC is not intended to focus sharp images, its mirror reflectors can be fabricated with less precision. Probably most important of all, the CPC does not need to track the sun to be operational, only occasional adjustments of tilt angles are needed, which greatly reduces the cost of the system. The present project addresses the design of a system that utilizes CPC to collect energy and to generate low quality steam for meeting industrial process heat (IPH) needs.

An examination of the nation's solar energy program reveals that the present project fits well into the Department of Energy's plan to commercialize solar energy in the industrial process heat sector. Solar IPH demonstration projects have been funded both by DOE and private industries as shown in Table 1 and Figure 1. Of those projects listed in the table, the great majority uses either a flat-plate collector or a parabolic trough concentrator to collect energy. CPC collectors have yet to make a penetration into this important segment of solar applications.

There are several constraints imposed on the design of the present system. Because of the use of receiver tubes inside a collector, in-situ boiling is handicapped due to the receiver tube strength, scaling problem and plumbing difficulties. On the other hand, the CPC collects energy from the sun that follows definite paths day in and day out. For the CPC to be economically competitive only occasional tilt adjustments are permitted, and the collector must be mounted along an east-west axis. This orientation limits the selection

Table 1: **Solar IPH Demonstration Projects**

Location	Process	Collectors	Owner	Status
Hot Water (60°-100°C)				
Sacramento CA	can washing	flat-plate & parabolic trough	Campbell Soup Co.	operational (April 1978)
Harrisburg, PA	concrete block curing	multiple reflector	York Building Products	operational (Sept. 1978)
La France, SC	textile dyeing	evacuated tube	Reigel Textile Corp.	operational (June 1978)
Hot Air				
Fresno, CA	fruit drying	flat-plate	Lamanuzzi & Pantaleo Foods	operational (May 1978)
Canton, MS	kiln drying of lumber	flat-plate	LaCour Kiln Services, Inc.	operational (Nov. 1977)
Decatur, AL	soybean drying	flat-plate	Gold Kist, Inc.	operational (May 1978)
Gilroy, CA	onion drying	evacuated tube	Gilroy Foods Inc.	construction
Low Temperature Steam (100°-180°C)				
Fairfax, AL	fabric drying	parabolic trough	WestPoint Pepperell	operational (Sept. 1978)
Sherman, TX	gauze bleaching	parabolic trough	Johnson & Johnson	construction
Pasadena, CA	laundry	parabolic trough	Home Cleaning & Laundry	construction
Bradenton, FL	orange juice pasteurization	evacuated tube	Tropicana Products, Inc.	construction
Intermediate Temperature Steam (180°-290°C)				
Mobile, AL	oil heating	parabolic trough	Ergon, Inc.	design
Dalton, GA	latex production	multiple reflector	Dow Chemical	design
Newberry Springs, CA	hectorite processing	parabolic trough	Nat'l Lead Industries	design
Hobbs, NM	oil refinery	parabolic trough	Southern Union Co.	design
San Antonio, TX	brewery	parabolic trough	Lone Star Brewing Co.	design
Henderson, NV	chlorine manufacturing	parabolic trough	Stauffer Chemical Co.	design
Ontario, OR	[illegible] processing	parabolic trough	Ore-Ida Co.	design
Privately Funded				
Youngstown, OH	aluminum anodizing	fixed half-parabolic	General Extrusions, Inc.	operational (Sept. 1977)
Jacksonville, FL	beer pasteurization	evacuated tube	Anheuser-Busch, Inc.	operational (Feb. 1978)

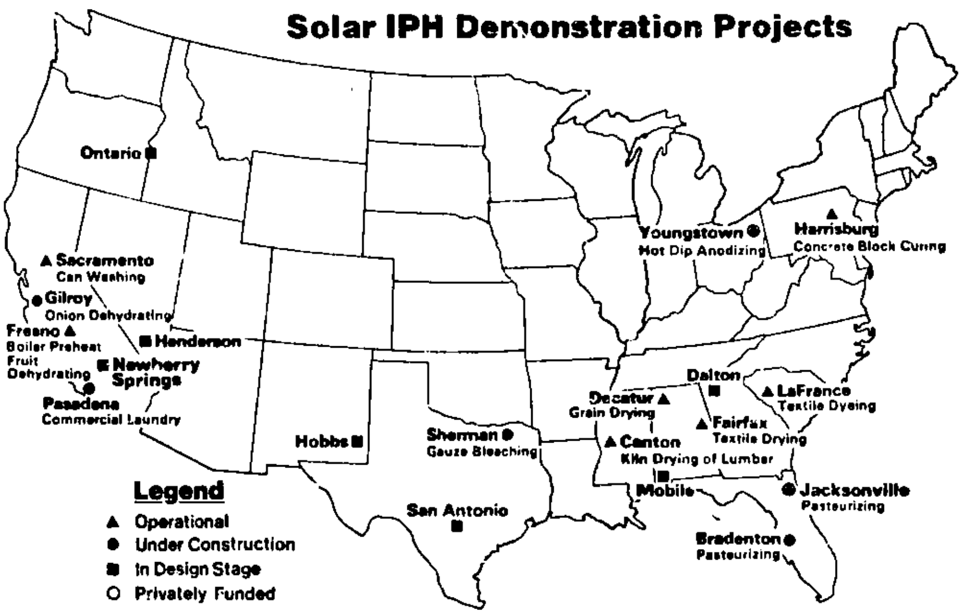

Fig. 1. Geographic Locations of Solar IPH Demonstration Projects

of heat transmission devices. Furthermore, the sun's energy is highly diluted. To make use of this dilute energy for a relatively energy concentrated application requires special design considerations. The design effort cannot follow the conventional steam generation practice and the project itself presents a real challenge to analysis.

The material presented in this report is divided primarily into two parts. In Section II the theoretical background for analysis is presented. This part consists of three subsections dealing separately with the optical and the thermal analyses of CPC and the heat pipe design theory. Of these three covered, since the optical analysis and the heat pipe design theory have been well documented in the literature [2-5], the materials given in this report are brief, and equations and theories given are limited only insofar as they are relevant to the present analysis and design of system. As to the thermal analysis of CPC collectors, there is a lack of thorough treatment in the literature. The ones given in [6-8] are incomplete and a full analysis appears in order. The thermal analysis part of this report will address the problem in detail.

Section III of this report presents a design of the system. For a detailed analysis of the system performance, two computer programs have been developed. They are used to simulate thermal processes of collectors in both collector and boiler loops in the system. The performance of heat pipes is also treated in detail in this section. These analyses permit sizing of the system to meet the need.

The computer programs have been included as appendices to this report. Detailed information is provided to show how these programs can be used for analysis.

It is not possible to make a transient system analysis in the present project, nor has the economic analysis been treated at this stage. They can be done in the future when specifications of the total system are identified. Nevertheless, the present project is complete to the level where specifications for major components (collectors, heat pipes, pumps) have been determined as given in this report. These informations will be instrumental to make system cost estimations if necessary.

II. ANALYSIS

The system under investigation is depicted in Figure 2. The CPC collector employs an evacuated tube receiver to intercept concentrated energy. The tube receiver has an evacuated space between the glass envelope and the receiver jacket. This evacuated space serves the purpose of eliminating the convective heat loss from the receiver. The receiver jacket is covered with a selective coating to raise its solar absorptance while minimizing its infrared emittance. The heat absorbed by the receiver jacket is transmitted to the fluid that is flowing inside the receiver tubing via the copper heat getter (fin) fitted inside the jacket wall. Two receiver tubings occupy the center space with only one tube spot welded to the getter; this is also the tube which delivers fluid to the collector, with the other tubing serving as a return passage of flow.

The collector utilizes a pair of compound parabolic reflectors to reflect sunlight onto the receiver. A clearance is built in between the lower surface of the receiver envelope and the mirror reflector. This clearance is provided to account for any misalignment that can happen to a long receiver tube under ends supported condition. This clearance together with the gap in the evacuated tube constitutes a loss to the intercepted energy as will be examined later.

1. Optical Analysis of CPC Collectors

It has been shown in the literature that the geometric concentration ratio (CR) of a CPC is [9]

$$CR = \frac{1}{\text{Sin } \Theta_{max}} \tag{1}$$

where Θ_{max} is the acceptance half-angle. Physically, because of the geometry

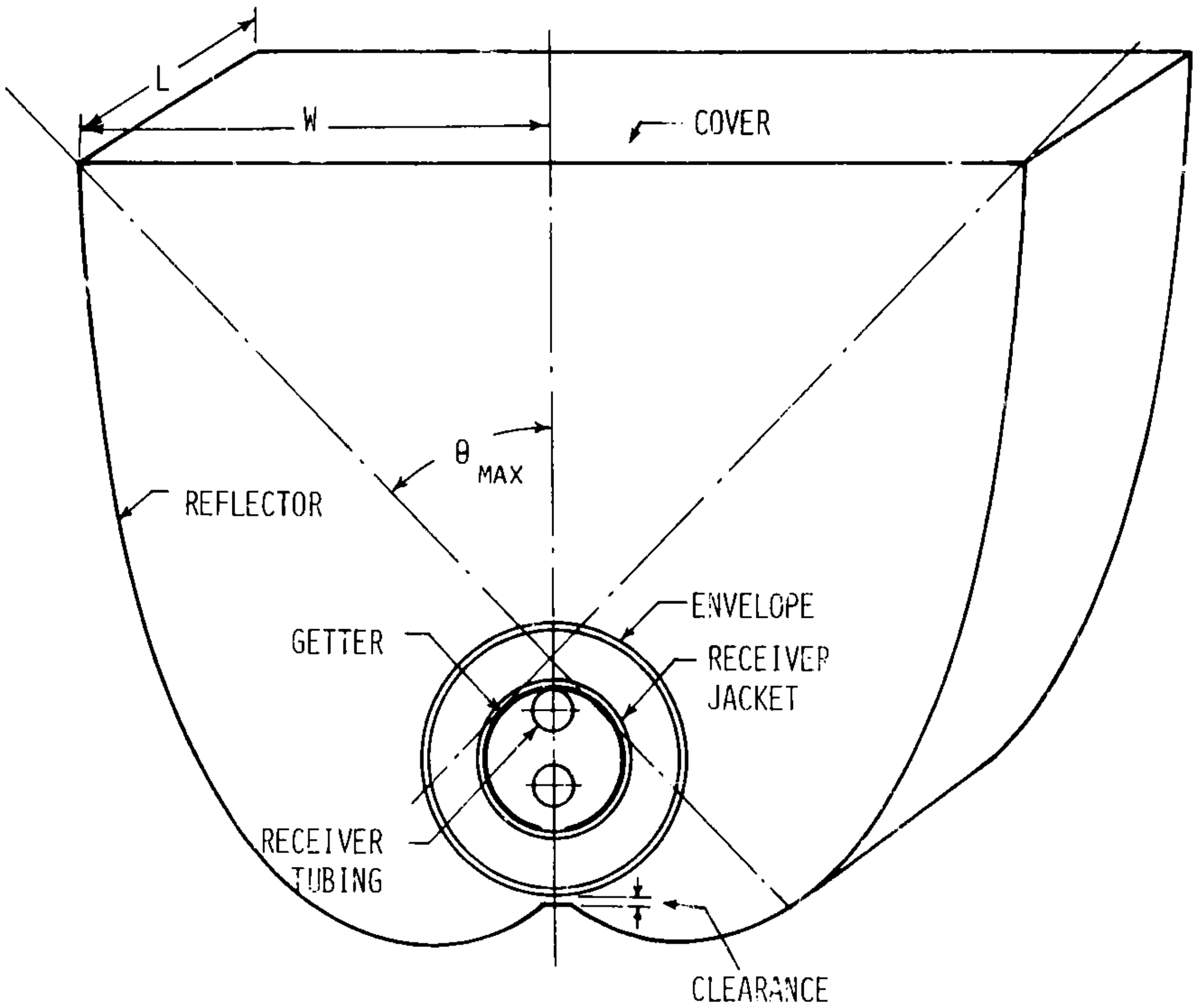

FIGURE 2. A SCHEMATIC DIAGRAM SHOWING A CPC COLLECTOR FITTED WITH A CTR TUBE

of the mirror reflector, any beam radiation incident on the collector cover that is contained within $|i| \leq \theta_{max}$ is able to reach the receiver. The concentration ratio used in this work is a geometric quantity and is defined on the basis of the total receiver area.

Unlike a flat-plate collector that is able to receive all the diffuse radiation that is incident on its aperture, the CPC's capability to intercept diffuse radiation is limited and is governed by the acceptance angle concept described above. Although the CPC cover can receive all the diffuse radiation, the fraction of energy that is transmitted through the cover and reaching the receiver is reduced by a factor of $(A_r/A_a) = (1/CR)$ for a two-dimensional CPC trough of interest in this study. By the same token, because of the geometry of the CPC mirror, all the energy leaving the receiver can, with the help of the mirror, reach the cover. Conversely, only a fraction (A_r/A_a) of the total energy leaving the cover can reach the receiver. This difference in shape factor relations gives rise to different formulations for energy exchanges as will be seen later in the analysis.

The reflection of energy in a CPC collector is also important. For incoming rays located in the central region of the aperture these rays undergo no reflection between the aperture and the receiver. This is not so, however, for edge rays, which undergo one or more reflections before reaching the receiver. The average number of reflections for all the rays filling the aperture can be found using a ray tracing technique, and its use greatly simplifies the analysis. The attenuation or loss of radiation due to mirror reflection can be expressed in terms of the average number of reflections $\bar{n}$ as

$$\text{Reflection Loss} = 1 - \rho_m^{\bar{n}} \qquad (2)$$

where ρ_m is the mirror reflectance. Values for $\bar{n}$ have been documented in the literature, for example [6,10]. In general, the average number of reflections is a function of the incidence angle, concentration ratio, receiver configuration and gap size. For most engineering designs the variation of $\bar{n}$ with the CPC incidence angle can be neglected for practical purposes [11].

As noted earlier, there is a gap between the receiver jacket and the mirror reflector. This gap represents a loss for the collector. Because of this gap the energy received by the absorber is reduced by a factor of p, given as [12]

$$p = 1 - \frac{g}{2\pi r_{r,o}} \tag{3}$$

where g is the total gap thickness (clearance plus evacuated gap); $r_{r,o}$ is the receiver jacket radius, see Figure 3.

2. Thermal Analysis of CPC Collectors

In order to simulate the thermal processes in the CPC, it is necessary to establish energy balance for various components in the collector. The interaction of the beam and diffuse radiation with the collector cover, receiver envelope and jacket will be treated first. A two-band model will be used in the analysis.

The beam radiation incident on the cover and absorbed by it can be expressed as

$$q_{b,a} = H_b(i) \left[\alpha_a(i) + \bar{\alpha}_a \tau_a(i) \bar{\rho}_e \, \rho_m^{2\bar{n}}\right] \frac{A_a}{A_r} \tag{4}$$

where the heat flux q has been written on the basis of a unit receiver-jacket area $A_r (= 2\pi r_{r,o} L)$, L, collector length. H_b represents beam radiation flux. α, ρ and τ denote the radiative properties in the solar spectrum and have their usual meanings (notations are defined in the Nomenclature). Subscripts a, e, m and r refer to cover, envelope, mirror and receiver, respectively.

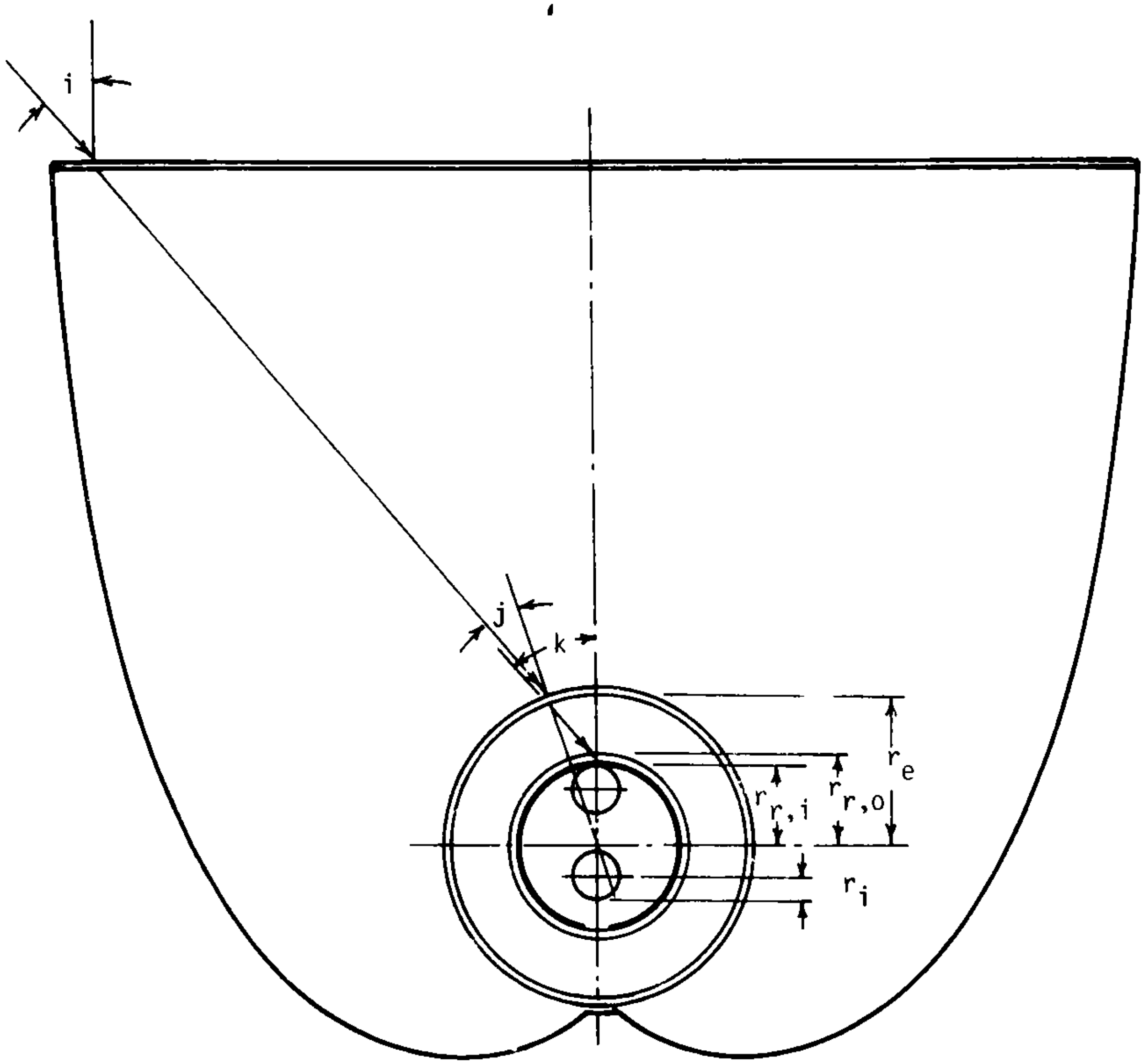

FIGURE 3. A DIAGRAM SHOWING INCIDENCE ANGLES AND RADII OF RECEIVER TUBE.

H_b, α_a and τ_a are functions of the beam incident angle i and have been so identified by appending parantheses. Overbars above properties designate mean values which remove the angular dependency. A_a is the aperture area of the collector, $A_a = 2wL$, w, half-width of aperture. The second term in the bracket accounts for the reflected energy from the envelope that is absorbed by the cover, a second-order effect.

The beam radiation transmitted through the cover and absorbed by the receiver envelope is

$$q_{b,e} = H_b(i)\tau_a(i)\rho_m^{\bar{n}}\left[\alpha_e(j) + \bar{\alpha}_e\bar{\rho}_e\bar{\rho}_a\rho_m^{2\bar{n}}\frac{A_e}{A_a} + \bar{\alpha}_e\bar{\rho}_r\tau_e(j)\right]\frac{A_a}{A_r} \qquad (5)$$

where $A_e = 2\pi r_e L$. The second term in the bracket accounts for that part of the beam radiation reflected from the envelope and rereflected from the cover and finally absorbed by the envelope. The third term takes into consideration the reflected energy from the receiver jacket that is incident on the envelope. This last contribution is small if the receiver jacket has a selective surface. They are included to account for second order effects.

The beam radiation transmitted through the cover and envelope and absorbed by the receiver jacket is

$$q_{b,r} = H_b(i)\tau_a(i)\rho_m^{\bar{n}}\tau_e(j)p\left[\alpha_r(k) + \bar{\alpha}_r\bar{\rho}_r\bar{\rho}_e\frac{A_r}{A_e}\right]\frac{A_a}{A_r} \qquad (6)$$

where p has been defined in Equation (3). The second term in the bracket accounts for the beam radiation that is not absorbed on its first impingement on the receiver but reflected from the jacket and rereflected from the envelope and eventually absorbed by the jacket, again a second order correction term.

The formulation for contributions of beam radiation is now complete; attention is now directed to the diffuse contributions. The diffuse radiation absorbed by the collector cover is

$$q_{d,a} = H_d\bar{\alpha}_a \left(1 + \bar{\tau}_a\bar{\rho}_e\rho_m^{2\bar{n}}\right)\frac{A_a}{A_r} \tag{7}$$

where H_d is the diffuse component of solar flux. Again the equation is written on the basis of a unit receiver-jacket area A_r. The second term in the parenthesis represents the second order effect due to reflection of diffuse radiation by the envelope and absorbed by the cover.

The contribution of diffuse radiation to the absorption in the envelope is

$$q_{d,e} = H_d\bar{\tau}_a\rho_m^{\bar{n}}\,\bar{\alpha}_e\left(1 + \bar{\rho}_e\bar{\rho}_a\rho_m^{2\bar{n}}\,\frac{A_e}{A_a} + \bar{\rho}_r\bar{\tau}_e\right)\frac{A_r}{A_a}\,\frac{A_a}{A_r} \tag{8}$$

The second and the third terms in the parenthesis have the same physical significance as the corresponding terms in Equation (5).

The diffuse contribution to absorption in the receiver jacket is

$$q_{d,r} = H_d\bar{\tau}_a\tau_e\alpha_r\rho_m^{\bar{n}}\,p\left(1 + \bar{\rho}_r\bar{\rho}_e\,\frac{A_r}{A_e}\right)\frac{A_r}{A_a}\,\frac{A_a}{A_r} \tag{9}$$

Once again, the second term in the parenthesis plays the same role as the corresponding term in Equation (6). p accounts for correction for gap loss.

Solar radiation incident on a CPC will raise the temperature of the collector, giving rise to an infrared energy exchange. This mode of heat transfer can be formulated in terms of surface infrared emittances and analyzed using an electric analog as follows.

For infrared exchange between the receiver jacket and the envelope, the radiant flux is

$$q_{IR,r/e} = \frac{\sigma\left(T_r^4 - T_e^4\right)}{\frac{1}{\varepsilon_r} + \frac{A_r}{A_e}\left(\frac{1}{\varepsilon_e} - 1\right)} \tag{10}$$

where σ is the Stefan-Boltzmann constant. The factor (A_r/A_e) for the second term in the denominator accounts for the view factor between the envelope and the receiver jacket. ε denotes the infrared emittance. This equation is written again on the basis of a unit receiver-jacket area.

The infrared exchange between the envelope and the collector cover is

$$q_{IR,e/a} = \frac{\left(\frac{A_e}{A_r}\right)\sigma\left(T_e^4 - T_a^4\right)}{\frac{1}{\varepsilon_e} + \frac{A_e}{A_a}\left(\frac{1}{\varepsilon_a} - 1\right)} \tag{11}$$

The heat loss from collector cover to sky is

$$q_{IR,a/s} = \varepsilon_a\,\sigma\left(T_a^4 - T_s^4\right)\frac{A_a}{A_r} \tag{12}$$

where the sky temperature T_s can be related to the ground-level ambient temperature T_b by [13]

$$T_s = T_b - 6 \tag{13}$$

In the above equation both T_s and T_b are in °C.

There are other modes of energy exchange inside the collector. The convective heat loss from the receiver envelope is

$$q_{c,e/a} = h_{e/a}\,\Delta T\,\frac{A_e}{A_r} \tag{14}$$

which is written again based on a unit receiver area. In the equation the convective coefficient $h_{e/a}$ is a function of temperatures and can be expressed in an empirical formula [14]

$$h_{e/a} = 1.32 \left(\frac{\Delta T}{2r_e}\right)^{1/4} \tag{15}$$

where ΔT and r_e are in units °C and m, respectively. This equation, having a 1/4 power temperature dependency, is inconvenient to use in the iterative solution. Attempt is thus made to linearilize this equation using the following:

$$h_{e/a} = 3.25 + 0.0085 \ \frac{T_e - T_a}{4 \ r_e} \tag{16}$$

where the sink temperature in the equation has been taken to be the mean of those of cover and envelope. Equation (16) provides a good approximation to the nonlinear equation (15) over the temperature range that is commonly encountered in CPC collectors, see Figure 4.

For convection loss from cover to ambient the equation to be used is

$$q_{c,a/b} = h_{a/b} \ (T_a - T_b) \ \frac{A_a}{A_r} \tag{17}$$

where T_b designates ambient temperature and $h_{a/b}$ is related to wind speed by [14]

$$h_{a/b} = 5.7 + 3.8V \tag{18}$$

where V is wind speed in units of m/s, $h_{a/b}$ in W/m^2 °C

It is noted that in a CPC collector the useful energy is extracted in the form of heat by flowing liquid inside the receiver tubing. If the contact resistance between the receiver jacket and the heat getter (fin) is ignored, the following equation can be written:

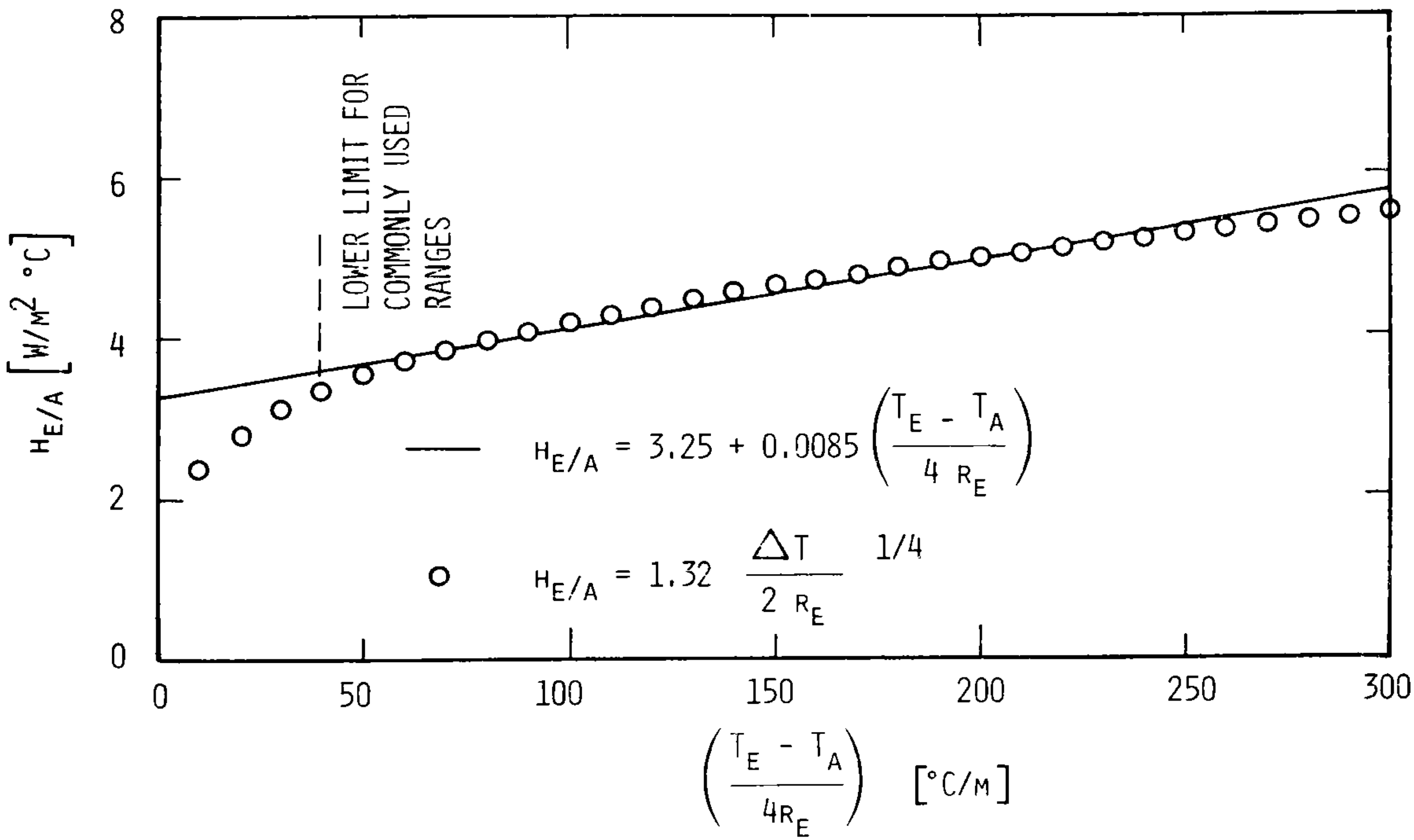

FIGURE 4. FREE CONVECTION COEFFICIENT FOR THE RECEIVER ENVELOPE

$$\dot{m}_c c_{pc}\left(T_o - T_i\right) = U_{r/1} A_r \left[T_r - \frac{\left(T_i + T_o\right)}{2}\right] = Q_u \tag{19}$$

where $\dot{m}_c c_{pc}$ refers to the thermal capacitance rate of the collector circulating fluid; subscripts i and o for T designate inlet and outlet sections respectively. A_r refers to the outside surface of the receiver jacket. The heat transfer coefficient $U_{r/1}$ accounts for both conduction across the receiver -jacket wall and convection inside the receiver tubing. It follows that

$$U_{r/1} = \left[\frac{r_{r,o}}{2.182\ k_f} + \frac{r_{r,o}\ \ln\left(r_{r,o}/r_{r,i}\right)}{k_g}\right]^{-1} \tag{20}$$

where subscripts f and g for k (thermal conductivity) refer to liquid and jacket wall, respectively. In the above equation the convective heat transfer between the fluid and the receiver tubing has been modeled using a constant heat flux condition. Its Nusselt number is [15]

$$Nu = 4.364 \tag{21}$$

The equations given above provide the basis for establishing energy balance for various components in the collector. An electric analog circuit depicting energy interactions between components can now be constructed as shown in Fig. 5. Based on this figure the energy balance equation for the collector cover under steady state condition can be derived as

$$q_{b,a} + q_{d,a} + q_{IR,e/a} + q_{c,e/a} - q_{IR,a/s} - q_{c,a/b} = 0 \tag{22}$$

where each term in this equation has been defined previously.

For the envelope the energy balance equation is

$$q_{b,e} + q_{d,e} + q_{IR,r/e} - q_{IR,e/a} - q_{c,e/a} = 0 \tag{23}$$

For the receiver jacket, the following energy balance relation can be established

$$q_{b,r} + q_{d,r} - q_{IR,r/e} - \frac{Q_u}{A_r} = 0 \tag{24}$$

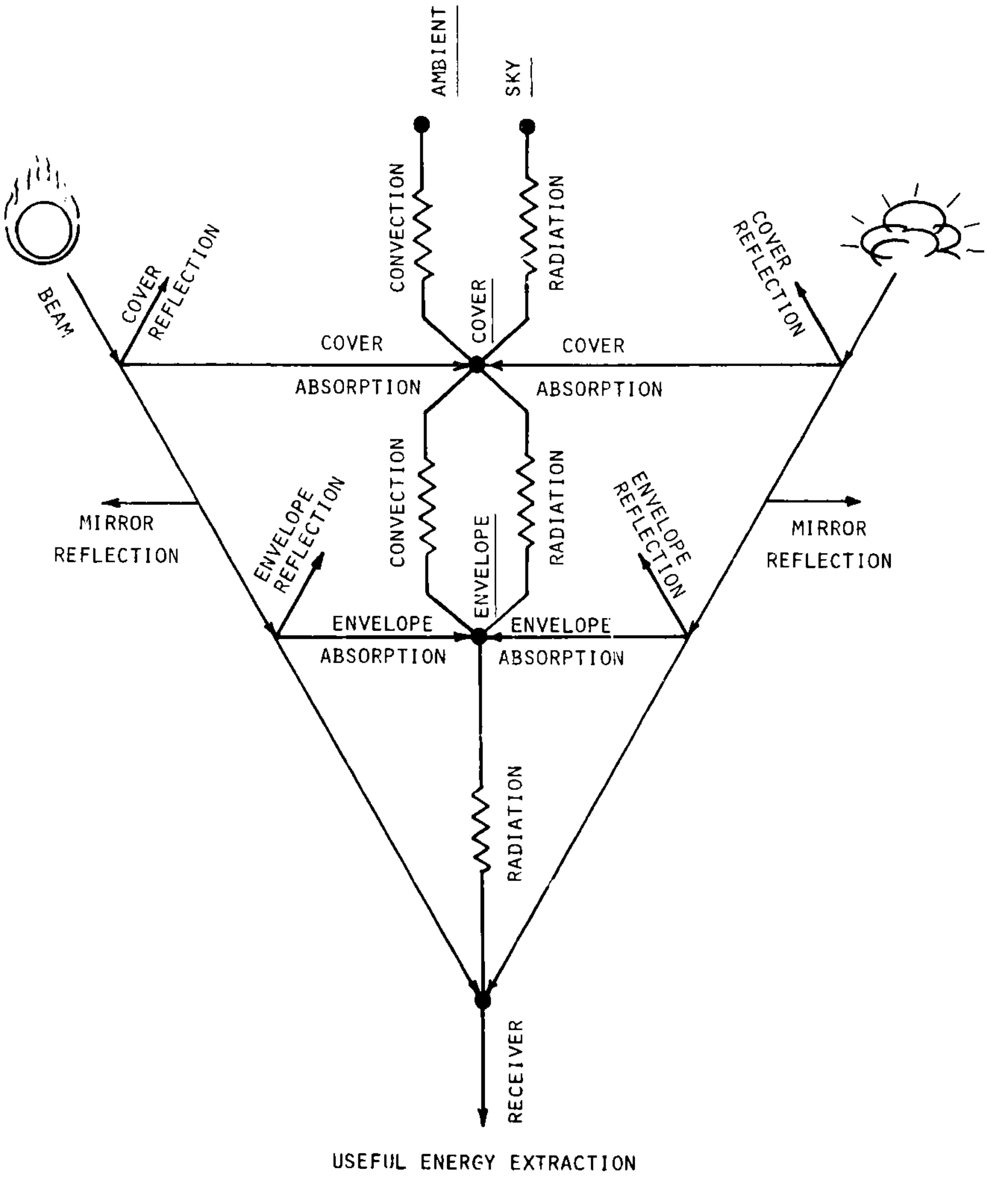

FIGURE 5. ELECTRIC ANALOG CIRCUIT FOR A CPC COLLECTOR

Note that there is no convective heat loss from the receiver jacket because the tube is evacuated.

Equations (22), (23) and (24) can be used together with (19) to form a set of four, nonlinear, algebraic equations to solve for four unkowns T_a, T_e, T_r and T_o if T_i is given. A computer program developed based on a combination of Newton-Raphson method and iteration solution is included as Appendix A to this report.

It is worthy of note that in the foregoing analysis the CPC mirror was not treated as a separate floating potential for the adiabatic surface role it plays. In fact, the computer data show that, because of the construction of the receiver, the vacuum surrounding the receiver jacket as well as the selective surface on the jacket provides good insulation of the receiver. As it turned out, the envelope has a fairly low temperature; and inclusion of the mirror analysis is certainly unnecessary for the collector.

Another question arises in connection with the rationale of omitting the back loss in the analysis. This can be justified by examining the models illustrated in Figure 6. The CPC mirror can be simulated as a flat radiation shield between the receiver envelope (e) and the back plate (f). For the system under consideration the heated surfaces are located above; convection is therefor negligible. The equivalent thermal resistances can be derived for various parts of heat flow and be formulated as shown. Tests have shown that the back loss is negligibly small for all CPC collectors.

The analysis presented above is complete in the sense that it can be used to predict collector performance and sizing collectors, if necessary. However, there will be a heat exchanger in the collector loop in the final design of systems. For such an arrangement the system performance will be a function of the heat exchanger penalty factor which is, in turn, a function of the heat

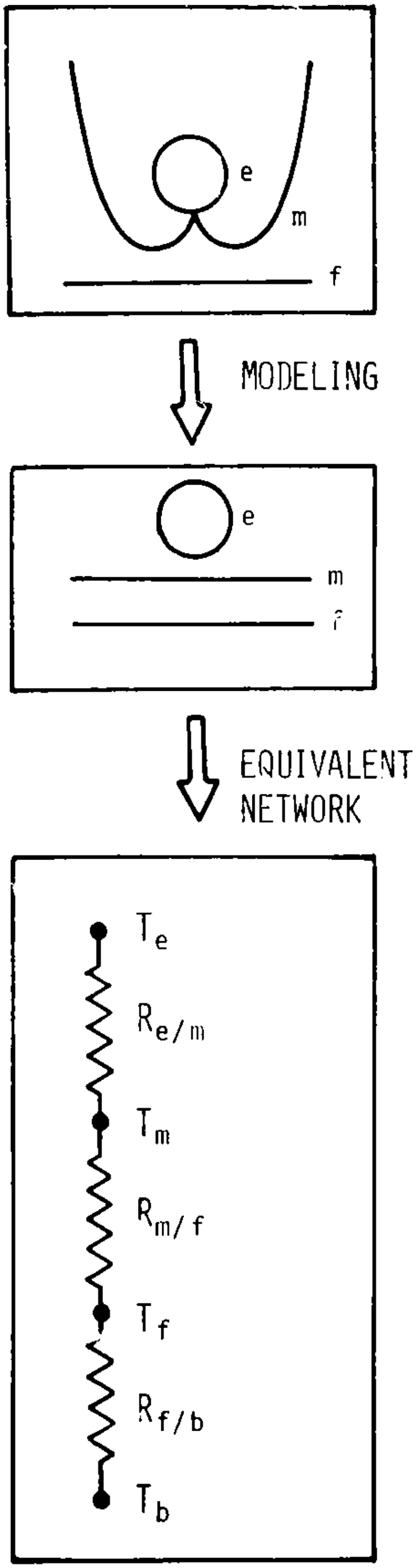

c ----- ENVELOPE

m ----- MIRROR

f ----- BACKPLATE

m ----- RADIATION SHIELD

F_{e-m} ----- SHAPE FACTOR, $F_{e-m} = 0.5$

$$R_{e/m} = \frac{\dfrac{\rho_e}{A_e \varepsilon_e} + \dfrac{2}{A_e} + \dfrac{\rho_m}{A_m \varepsilon_m}}{4\sigma \left(\dfrac{T_e + T_m}{2} \right)^3}$$

$$R_{m/f} = \frac{\dfrac{\rho_m}{A_m \varepsilon_m} + \dfrac{1}{A_m} + \dfrac{\rho_f}{A_m \varepsilon_f}}{4\sigma \left(\dfrac{T_m + T_f}{2} \right)^3}$$

$$R_{f/b} = \frac{1}{hA_f}$$

FIGURE 6. MODELING OF HEAT TRANSFER THROUGH THE BACK PLATE OF A CPC COLLECTOR

removal factor, among others. A separate analysis is thus in order to derive this heat removal factor.

The analysis to be developed follows the Hottel-Whillier-Woertz-Blizz (HWWB) formulation that was originally derived for analyzing flat-plate collectors [16-18]. The useful energy extracted from the CPC collector can be written as

$$Q_u = H_t \bar{\tau}_a \rho_m^{\bar{n}} \bar{\tau}_e \bar{\alpha}_r p A_a - U_L A_r (T_r - T_b) \tag{25}$$

where H_t is the total solar flux defined as

$$H_t = H_b(i) + H_d \tag{26}$$

U_L is the receiver surface loss coefficient.

Equation (25) appears to be quite simple. However, the analysis does not account for multireflections as what has been afforded in the previous analysis. Hence, using Equation (25) to predict useful heat gain could result in an underestimation because of the omission of second order effects. This point can be verified by data as will be shown later in this report.

Equation (25) can be recast in a simpler form by introducing

$$S' = H_t \bar{\tau}_a \rho_m^{\bar{n}} \bar{\tau}_e \bar{\alpha}_r p \frac{A_a}{A_r} \tag{27}$$

thus giving

$$Q_u = A_r \left[S' - U_L(T_r - T_b)\right] \tag{28}$$

Another way to write Q_u equation is to express Q_u in terms of the mean fluid temperature T_f inside the receiver tubing. If both conductive resistance inside the receiver-jacket wall and the convective resistance inside the receiver tubing are accounted for, there is derived

$$Q_u = F'A_r \left[S' - U_L \left(T_f - T_b\right)\right] \tag{29}$$

where F′ is the ratio of the overall loss coefficient to the receiver surface loss coefficient, given as

$$F' = \frac{U_o}{U_L} = \frac{\left(1/U_L\right)}{\left(1/U_L\right) + r_{r,o} \ln\left(r_{r,o}/r_{r,i}\right)/k_g + r_{r,o}/\left(r_i h_i\right)} \tag{30}$$

Physically, F′ represents the ratio of the useful heat gain to the heat gain of a hypothetical case if the receiver jacket surface had been at the fluid "mean" temperature.

A third way to write Equation (28) is to introduce the heat removal factor defined as

$$F_R = \frac{G\ c_{pc}(CR)}{U_L} \left[1 - \exp\left(- \frac{U_L F'}{G\ c_{pc}(CR)}\right)\right] \tag{31}$$

where $G = \dot{m}_c/A_a$. This permits rewriting Q_u as

$$Q_u = F_R A_r \left[S' - U_L(T_i - T_b)\right] \tag{32}$$

Note that the T_r in Equation (28) [or T_f in Equation (29)] has been changed to T_i in the above equation. Physically, F_R can be interpreted in a similar way as F′. More specifically, F_R represents the ratio of the useful heat gain to the heat gain if the receiver jacket had been at the "inlet" fluid termperature.

The analysis developed above follows the HWWB formulation for flat-plate collectors. The formulations given here are more general in the sense that, when

$$(CR) = \rho_m^{\bar{n}} = \bar{\tau}_e = p = 1 \tag{33}$$

the three Q_u equations given above can all be reduced to the similar equations for flat-plate collectors.

Another point of interest is that, if F_R/F' is plotted versus $Gc_{pc}/F'U_L$, a family of curves is obtained as shown in Figure 7. For CPC collectors the curves reach the asymtotic value of unity earlier than flat-plate collectors (labeled CR = 1). The small U_L typical for a CPC collector will also raise the value of $Gc_p/F'U_L$ which is plotted as abscissa in the figure. These cumulative effects will lead to a higher F_R, a desirable feature from the heat gain point of view.

The Q_u equations [Equations (28), (29) and (32)] derived above all share a common simplification - the energy absorbed in the cover and the receiver envelope has been ignored. In fact, the equivalent thermal circuit is the one shown in the left of Figure 8. A way to improve this analysis is to include the absorption as shown in the right of the figure. Physically, absorption in the cover and envelope will raise the temperature of these components, thereby reducing the receiver losses. Consequently, the useful energy output from the collector can also be increased. The derivation is quite tedious, but the result can be presented in a relatively simple formula as follows:

$$Q_u = F_R A_r \left\{ S' + H_t \left[\bar{\tau}_a \left(1 - \bar{\tau}_e\right) \frac{U_L A_r}{U_{e/a} A_e} + \left(1 - \bar{\tau}_a \bar{\tau}_e\right) \frac{U_L A_r}{U_{a/b} A_a} \right] - U_L (T_i - T_a) \right\} \quad (34)$$

where

$$U_{r/e} = \frac{\sigma\left(T_r^2 + T_e^2\right)\left(T_r + T_e\right)}{\dfrac{1}{\varepsilon_r} + \dfrac{A_r}{A_e}\left(\dfrac{1}{\varepsilon_e} - 1\right)} \quad (35)$$

$$U_{e/a} = \frac{\sigma\left(T_e^2 + T_a^2\right)\left(T_e + T_a\right)}{\dfrac{1}{\varepsilon_e} + \dfrac{A_e}{A_a}\left(\dfrac{1}{\varepsilon_a} - 1\right)} + h_{e/a} \quad (36)$$

$$U_{a/b} = \varepsilon_a \sigma \frac{T_a^4 - T_s^4}{T_a - T_b} + h_{a/b} \quad (37)$$

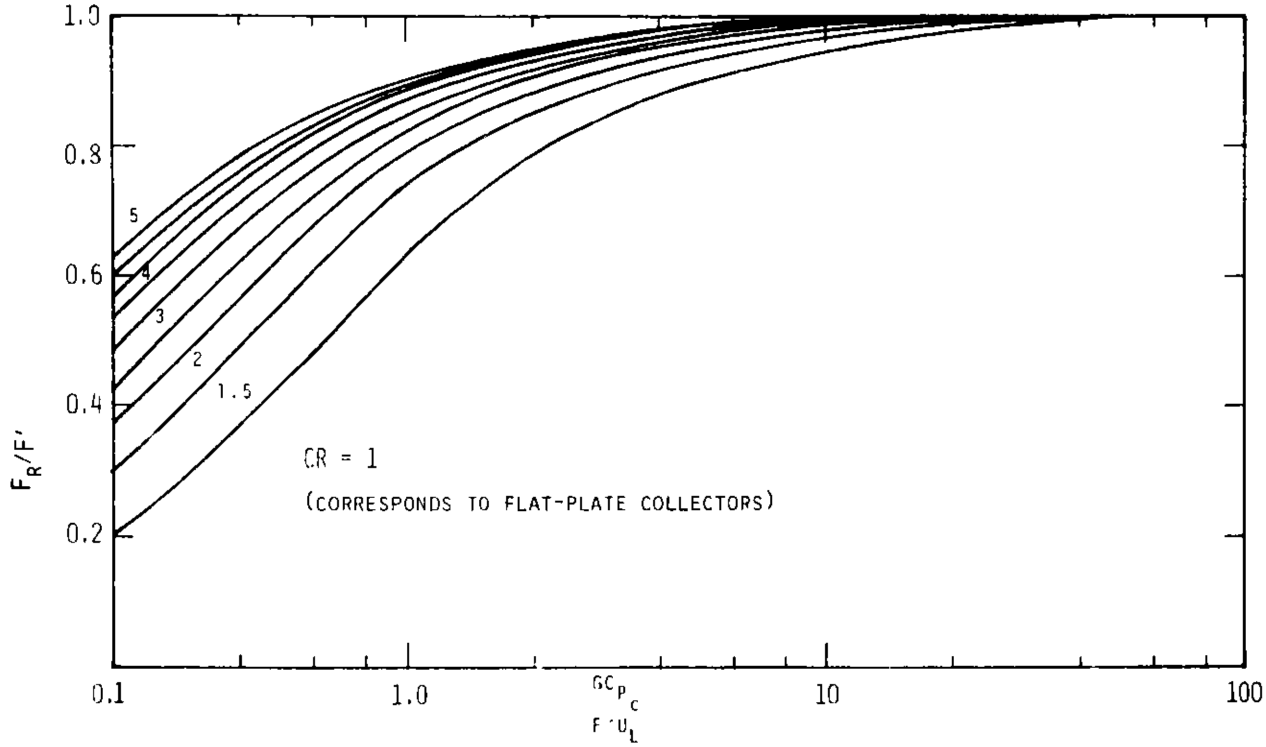

FIGURE 7. F_R/F' CURVES FOR CPC COLLECTORS

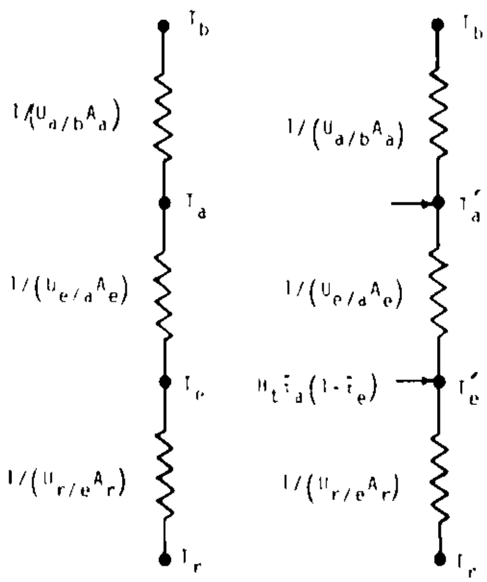

FIGURE 8. EQUIVALENT ELECTRIC CIRCUITS FOR A SIMPLIFIED THERMAL ANALYSIS OF CPC COLLECTORS

$$U_L = \frac{1}{A_r}\left(\frac{1}{U_{r/e}A_r} + \frac{1}{U_{e/a}A_e} + \frac{1}{U_{a/b}A_a}\right)^{-1} \tag{38}$$

A comparison between Equations (32) and (34) reveals that the improvement in the analysis results in the appearance of the correction (second) term in the braces of Equation (34).

It is now possible to write four efficiency equations based on Equations (28), (29), (32) and (34). By dividing Q_u by H_tA_a, it can be derived that

$$\eta = \eta_o - \frac{U_L}{H_t(CR)}\left(T_r - T_b\right) \tag{39}$$

$$\eta = \eta_o F' - \frac{U_L F'}{H_t(CR)}\left(T_f - T_b\right) \tag{40}$$

$$\eta = \eta_o F_R - \frac{U_L F_R}{H_t(CR)}\left(T_i - T_b\right) \tag{41}$$

$$\eta = \eta_o F_R + F_R F_A - \frac{U_L F_R}{H_t(CR)}\left(T_i - T_b\right) \tag{42}$$

where η_o is optical efficiency defined as

$$\eta_o = \bar{\tau}_a \, \rho_m^{\bar{n}} \, \bar{\tau}_e \, \bar{\alpha}_r \, \mu \tag{43}$$

F_A in Equation (42) can be termed as an enclosure absorption factor, defined as

$$F_A = \frac{1}{(CR)}\left[\bar{\tau}_a\left(1 - \bar{\tau}_e\right)\frac{U_L A_R}{U_{e/a}A_e} + \left(1 - \bar{\tau}_a\bar{\tau}_e\right)\frac{U_L A_R}{U_{a/b}A_a}\right] \tag{44}$$

In addition, based on the actual tests of CPC collectors, one can measure $\dot{m}_c$, T_i, T_o and H_t and derive another efficiency equation as follows.

$$\eta = \frac{\dot{m}_c C_{pc}\left(T_o - T_i\right)}{H_t A_a} \tag{45}$$

Clearly, Equations (39), (40) and (41) are all based on the same basic formulation and are expected to yield identical results. η calculated based on Equation (42) should be slightly higher because of the consideration of enclosure absorptions in the analysis. On the other hand, if Equation (45) is used for prediction, in which T_o is "computed" based on the solution of simultaneous nonlinear equations given earlier, this computed η will be the highest of all. This is because of the fact that the second order effects including multireflections and absorptions have all been included in this final analysis.

The analysis of CPC collector is now complete; attention is now directed to the penalty resulting from the use of a heat exchanger in the collector loop.

DeWinter [19] has derived a heat-exchanger penalty factor defined as the ratio of the actual heat gain for a system installed with a heat exchanger to a hypothetical heat gain if the exchanger was not there. The analytical expression for the penalty factor is

$$F_x = \frac{1}{1 + \frac{F_R U_L}{Gc_{pc}} \left[\frac{(\dot{m}c_p)_c}{(\dot{m}c_p)_{min}\ \varepsilon_x} - 1 \right]} \tag{46}$$

where $(\dot{m}c_p)_c$ refers to the heat capacitance rate for the circulating fluid in the collector. $(\dot{m}c_p)_{min}$ refers to the smaller of the two fluids circulating in the heat exchanger. ε_x is the heat exchanger effectiveness, which is related to the overall heat transfer coefficient $(UA)_x$ in the heat exchanger according to:

$$\varepsilon_x = \frac{(UA)_x/(\dot{m}c_p)_{min}}{1 + (UA)_x/(\dot{m}c_p)_{min}} \tag{47}$$

A counterflow heat exchanger is most effective from the heat transfer point of view. e_x for a counterflow heat exchanger is plotted in Figure 9. The heat exchanger penalty factor is plotted in Figure 10. As expected, a large $(UA)_x$ will raise e_x which, in turn, diminishes the penalty using a heat exchanger.

3. Heat Pipe Design Theory

Heat pipes will be used to transmit heat in the boiler in the final design of systems. Heat pipe design theory is briefly reviewed here.

The selection of materials in the heat pipe design is governed by several considerations. In order to maximize the heat that can be carried by a heat pipe the working fluid should be selected that has a high liquid transport factor N_ℓ, defined as

$$N_1 = \frac{\xi \rho_1 h_{fg}}{\mu_1} \tag{48}$$

where ξ refers to the surface tension coefficient, ρ density, μ dynamic viscosity and h_{fg} heat of vaporization. Subscript 1 refers to liquid for all properties. On the other hand, to minimize the temperature drop across the wick material the working fluid should be selected that has a large liquid conductance factor defined as

$$N_{k_1} = k_1 N_1 \tag{49}$$

where k_1 denotes the thermal conductivity of liquid.

The selection of wick material is important to the development of capillary pressure in the wick. To raise the heat transport capability, the wick must have large permeability K defined as

$$K = \frac{2 \phi r_h^2}{(f_1 Re_1)} \tag{50}$$

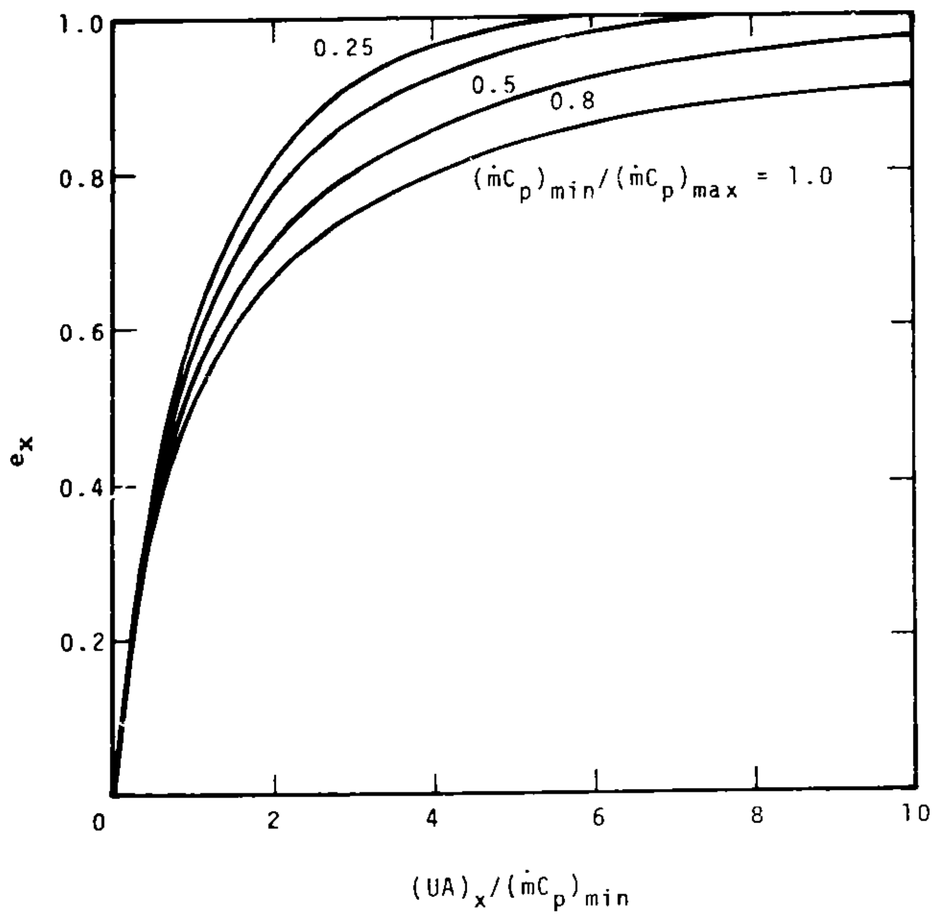

FIGURE 9. HEAT EXCHANGER EFFECTIVENESS CURVES

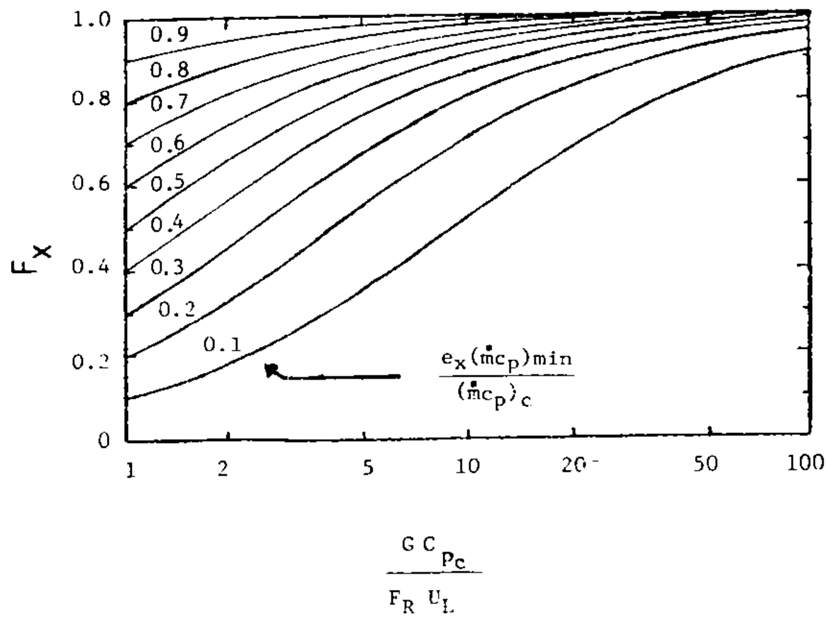

FIGURE 10. HEAT EXCHANGER PENALTY CURVES

where ϕ is the wick porosity, r_h is the hydraulic radius of wick. Drag coefficient f_l and Reynolds number Re_l in the above equation are given respectively as

$$f_l = \frac{2\,\tau_l}{\rho_l\,V_l^2} \tag{51}$$

$$Re_l = \frac{\rho_l\,V_l\,2r_h}{\mu_l} \tag{52}$$

where τ_l is the shear stress at the liquid-solid (wall) interface, V_l is the liquid velocity in wick. It is noted that, while the capillary pumping pressure is inversely proportional to the pore size, the liquid-flow resistance is inversely proportional to the wick permeability.

In choosing materials for heat pipe containers, consideration must be given to the compatibility between the working fluid and pipe wall. Only tests can show if two media are truly compatible. For the present application of heat pipes in a CPC collector, the heat pipe weight is of minor importance. However, the pipe wall conductance is important and the wall material chosen must have high conductance factor, defined as

$$N_{k_p} = k_p\,s_u \tag{53}$$

where k_p denotes the thermal conductivity of the pipe wall. s_u is the ultimate tensile stress of the wall material. A strong material having a large thermal conductivity will lead to a large N_{k_p}. Such a heat pipe will result in a small temperature drop for heat flow.

For heat pipes operating under elevated temperatures and vapor pressures the strength of the pipe container must be given special consideration. The ASME code for unfired pressure vessels should be consulted in the design of pipe containers. According to this code, the maximum allowable stress in the wall is taken to be one-fourth of the material ultimate strength (s_u) at the same temperature. For a circular heat pipe, this stress limitation permits a design of pipe radius as follows

$$\frac{r_{p,i}}{r_{p,o}} = 1 - \frac{4(\Delta p)}{s_u} \tag{54}$$

where Δp designates the pressure difference across the pipe wall. Equation (54) is derived based on a static force balance and is valid if the wall thickness is less than 10% of the diameter of the pipe.

In a like manner, the end cap thickness t can be calculated. For a heat pipe fitted with a flat cap, the cap thickness can be calculated using

$$t = \left[\frac{2(\Delta p)r_{p,o}^2}{s_u}\right]^{1/2} \tag{55}$$

Probably one of the most important considerations in the design of heat pipes is to determine if the designed heat pipe is capable of carrying the heat load as intended. It is common practice to evaluate this heat transfer limit using a capillary pressure analysis. Once this limit is found, the heat pipe must be further checked to see if this capillary limitation stays within the heat loads computed at other operating limitations. Specifically, heat loads at sonic limitation, entrainment limitation and boiling limitation must be separately computed and the smallest load found to be considered the operating limit of the pipe. In the paragraphs that follow, these limitations will be individually analyzed. The capillary limitation is treated first.

One of the functions a wick performs is to develop a capillary pressure inside the pipe such that the capillary pumping pressure is greater than the sum of all viscous pressure losses and gravity losses. For a heat pipe operating in the heat pipe mode the capillary limitation on heat load can be evaluated using

$$\int_0^{L_t} Q \, d\chi = \frac{p_c - p_s}{F_1 + F_v} \tag{56}$$

where Q refers to the "axial" heat flow, L_t is the total length of the heat pipe. p_c is the maximum capillary pressure, which is a function of the surface tension coefficient and the effective capillary radius. The capillary pressure varies with the wick design. p_s in Equation (56) designates the static pressure. For a tilted heat pipe as shown in Figure 11, this hydrostatic pressure can be expressed as

$$p_s = \rho_1 \, g \left(2r_{p,i} \cos \psi \pm L_t \sin \psi \right) \tag{57}$$

where ϕ is the tilt angle. The sign in front of the body force is determined by its direction and is positive (negative) if the direction of the component of gravity along the heat pipe is opposite to (the same as) the direction of integration of Q [Equation (56)].

F_1 and F_v in Equation (56) designate liquid and vapor frictional coefficients. F_1 is related to wick permeability K [Equation (50)] by

$$F_1 = \frac{\mu_1}{K \, A_w \, h_{fg} \, \rho_1} \tag{58}$$

where A_w denotes the wick cross-sectional area. This frictional coefficient accounts for the friction the liquid experiences when it is flowing inside the wick and was derived on the basis of a control volume analysis of force balance on the wick material.

For a screen-mesh wick of interest in this project, the permeability K can be related to wick porosity ϕ by

$$K = \frac{d_m^2 \, \phi}{122(1-\phi)^2} \tag{59}$$

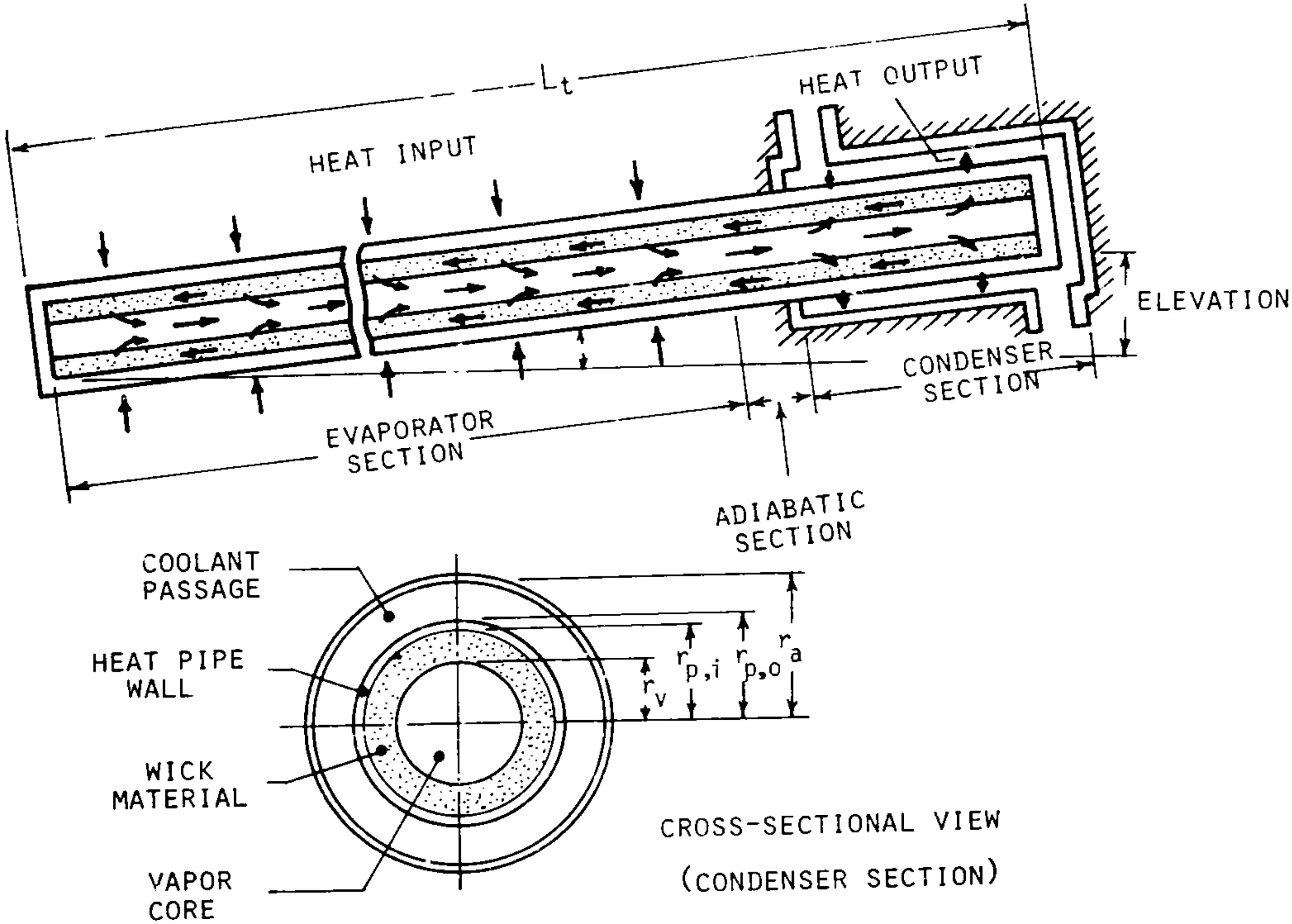

FIGURE 11. A SCHEMATIC DIAGRAM SHOWING HEAT PIPE OPERATIONS AND VARIOUS DIMENSIONS

This porosity is related to the mesh number N and mesh-wire diameter d_m by

$$\phi = 1 - \frac{1.05\pi N d_m}{4} \tag{60}$$

F_v in Equation (56) is the counterpart of F_ℓ in the same equation. This F_v accounts for frictions in the vapor core. For conventional heat pipes operating at cryogenic or moderate temperatures, the vapor flow in the core is mostly incompressible (Mach number ≤ 0.2) and laminar (Reynold number $\leq 2{,}300$). Under these conditions, F_ℓ and F_v are independent of Q. This not only makes the derivation of Equation (56) possible, but also leads to a smaller vapor temperature gradient desirable from the heat transfer point of view. For incompressible laminar flow inside a circular core, F_v can be expressed as

$$F_v = \frac{8\mu_v}{\pi r_v^4 \rho_v h_{fg}} \tag{61}$$

where Hagen-Poiseuille solution for laminar flow has been used in the simplification.

For a heat pipe exposed to uniform heat fluxes, the left hand side of Equation (56) can be related to the maximum axial heat flow as follows.

$$\int_o^{L_t} Q dx = \frac{L_e + 2L_a + L_c}{2} Q_{max,capillary} \tag{62}$$

where L_e, L_a and L_c designate evaporator, adiabatic section and condenser lengths, respectively. Equation (62) can be used together with Equation (56) to find the heat load at capillary limitation.

The heat pipe designed on the basis of the capillary limitation must be tested of its heat carrying capacity at sonic limitation. This sonic limitation is the condition when the vapor velocity at the evaporator exit reaches a Mach number of unity. The vapor flow inside a heat pipe resembles in many ways flows inside a convergent-divergent nozzle. Once this "chocking" occurs, a further decrease of the sink temperature will not result in a further increase of the total heat flow. Levy's equation can be used to predict this sonic limitation, which is given as

$$Q_{max,sonic} = A_v \rho_o h_{fg} \left[\frac{\gamma_v R_v T_o}{2(\gamma_v + 1)}\right]^{1/2} \tag{63}$$

where γ_v is the specific heats ratio for vapor, R_v is the vapor gas constant. Subscript o for ρ and T refers to a stagnation condition.*

The entrainment limit deals with a total different state of affairs. Inside the heat pipe both vapor and liquid are moving in opposite directions. Because of the low density and, therefore, the high velocity of vapor, liquid at the wick surface tends to be torn apart by vapor and entrained in the vapor stream. This results in an added circulation and upsetting the flow. Eventually the returned liquid may fail to catch up with the vapor flow rate; dry-out then occurs.

The heat load at the entrainment limitation can be derived by equating the shear force at the liquid-vapor interface and the surface force that holds the liquid in place and expressed as

$$Q_{max,\ entrainment} = A_v h_{fg} \left(\frac{\xi \rho_v}{2 r_{h,pores}}\right)^{1/2} \tag{64}$$

where $r_{h,pores}$ refers to the hydraulic radius of the wick surface pores. This radius is equal to half of the wire spacing for screen-mesh wicks.

---

*Readers are cautioned against the difference between the stagnation condition in fluid dynamics and the stagnation condition in testing of solar collectors. The former is referred to in Equation (63).

The boiling limitation also deals with the dry-out phenomenon but in a different perspective. In heat pipe operations, the liquid pressure at the evaporator is equal to the difference between the saturation pressure of the wick fluid at the temperature of the liquid-vapor interface and the capillary pressure at the same location. The saturation vapor pressure is therefore higher than the liquid pressure. Under high heat flux conditions, vapor bubbles may form in the evaporator wick. These bubbles obstruct the flow and may cause hot spots in pipes. The boiling limitation addresses this operation problem and the following equation can be used to predict the heat load.

$$Q_{max,\ boiling} = \frac{4\pi\ L_e\ k_e\ T_v\ \xi}{r_n\ \rho_v\ h_{fg}\ \ell n\left(r_{p,i}/r_v\right)} \tag{65}$$

where k_e denotes the effective thermal conductivity of the wick material. For the wire-mesh wick of interest in this study, k_e can be formulated as

$$k_e = \frac{k_\ell \left[(k_1 + k_w) - (1 - \phi)(k_1 - k_w)\right]}{(k_1 + K_w) + (1 - \phi)(k_1 - k_w)} \tag{66}$$

where k_1 and k_w refer to liquid and wick thermal conductivities, respectively. r_n in Equation (66) designates critical radius for nucleate boiling. For a conservative design, this radius can be taken as

$$r_n = 2.54 \text{ X } 10^{-7} \text{ m (or } 10^{-5} \text{ in.)} \tag{67}$$

The theory for design of heat pipes is now complete. A final note is in order to formulate the overall heat transfer coefficient between the evaporator and the condenser section of the heat pipe. This coefficient is needed later to evaluate the performance of CPC collectors fitted with heat pipe.

For the heat pipe shown in Figure 11, the overall heat transfer coefficient between the evaporator surface and the condenser surface can be expressed, based on the pipe's cross-sectional area, as

$$U_p = \left(R_{p,e} + R_{w,e} + R_v + R_{w,c} + R_{p,c} \right)^{-1} \tag{68}$$

where $R_{p,e}$, $R_{w,e}$, R_v, $R_{w,c}$ and $R_{p,c}$ designate thermal resistances in the evaporator side of the pipe wall, evaporator side of the wick material, vapor core, condenser side of the wick material and condenser side of the pipe wall, respectively. They can be separately formulated as follows.

$$R_{p,e} = \frac{r_{p,o}^2 \ln (r_{p,o}/r_{p,i})}{2\ L_e\ k_p} \tag{69}$$

$$R_{w,e} = \frac{r_{p,o}^2 \ln (r_{p,i}/r_v)}{2\ L_e\ k_e} \tag{70}$$

$$R_v = \frac{\pi r_{p,o}^2\ T_v\ (p_{v,e} - p_{v,c})}{\rho_v\ h_{fg}\ Q} \tag{71}$$

$$R_{w,c} = \frac{r_{p,o}^2 \ln (r_{p,i}/r_v)}{2\ L_c\ k_e} \tag{72}$$

$$R_{p,c} = \frac{r_{p,o}^2 \ln (r_{p,o}/r_{p,i})}{2\ L_c\ k_p} \tag{73}$$

where k_e is the effective thermal conductivity of the wick material, which has been defined earlier as Equation (66). Equation (71) was derived on the basis of the Clausius-Clapeyron equation. The vapor pressure drop between the evaporator and the condenser can be related to the axial heat flow. For a laminar incompressible flow of vapor with a negligible dynamic effect and under the condition when the pipe wall is exposed to a uniform heat flux, this pressure drop can be expressed as

$$p_{v,e} - p_{v,c} = F_v\ Q\ \frac{L_e + 6L_a + L_c}{6} \tag{74}$$

Substitution of Equation (74) into (71) yields

$$R_v = \frac{\pi r_{p,o}^2 \; T_v \; F_v \; (L_e + 6L_a + L_c)}{6\rho_v \; h_{fg}} \tag{75}$$

Finally, attention is directed to the convective coefficient on the surface of the condenser. For the arrangement shown in Figure 11, flow is confined inside an annulus at the condenser section, and the outside surface of the heat exchanger is insulated. Lundberg, et al. [20] have studied the problem analytically. For the system given, the Nusselt number at the outside surface of the annulus is zero, while that for the inside surface,

$$Nu_i = \frac{h_c \; D_a}{k} = 5.663 \tag{76}$$

where D_a is hydraulic diameter for the annulus, defined as

$$D_a = 2 \; (r_a - r_{p,o}) \tag{77}$$

Equation (76) can be used together with Equation (68) to develop a U equation for heat transfer from the surface of the evaporator to the fluid at the condenser side of the heat exchanger. Once this U is found, the thermal analysis given in the preceding subsection can be reused to determine the system performance for CPC collectors fitted with heat-pipe receivers.

III. DESIGN OF SYSTEM AND PREDICTION OF PERFORMANCE

A design of the total system is shown in Figure 12. The design meets all the constraints described in the INTRODUCTION section of this report. It also possesses several features as discussed below.

The total steam-generation system is divided into two loops: the collector loop and the boiler loop. In the collector loop the CPC collectors are fitted with concentric tube receivers (CTR). Collectors of this design have been extensively tested with several types of CTR receivers here at Argonne, and their performance records have been established. Because of the use of a heat exchanger (preheater) in this loop, antifreezes can be used for collector circulation. This arrangement alleviates the collector freezing problem while it raises the boiling point of the circulation liquid as desired. A summary of glycol properties is listed in Table 2. 80% by weight of ethylene glycol in an aqueous solution has been found to be satisfactory for the present project.

The use of a heat exchanger in the collector loop also permits the use of a more fragile CTR (e.g., Owen-Illinois tubes) for heat collection. As long as the tubings in the heat exchanger are leak-proof, the slightly pressurized water in the boiler loop is separated from the circulating antifreeze and will not endanger the safe operation of the tubes.

In the boiler loop water leaving the preheater enters an array of CPC collectors that are fitted with heat pipes. In these collectors heating takes place outside the heat pipe; scaling becomes of minor concern. These heat pipes will heat the circulating water "near" boiling at elevated pressures. Then, once the water is discharged through a throttling valve, part of the water will flash into steam. The flash boiler serves primarily as a separator to direct

Table 2. Thermodynamic Properties of Aqueous Solutions of Glycols (22)

	Ethylene Glycol (80% by Weight)	Diethylene Glycol (80% by Weight)	Triethylene Glycol (80% by Weight)	Propylene Glycol (80% by Weight)
Thermal Conductivity at 120°C	0.2768	0.2595	0.2422	0.2249 W/m°C
Constant Pressure Specific Heat at 120°C	3226	3140	3120	3475* J/kg°C
Freezing Point	-45	-37*	-38.5	(not available)
Boiling Point	124	117	113	119
Specific Gravity	1.022	1.032	1.037	0.962

*by extrapolation

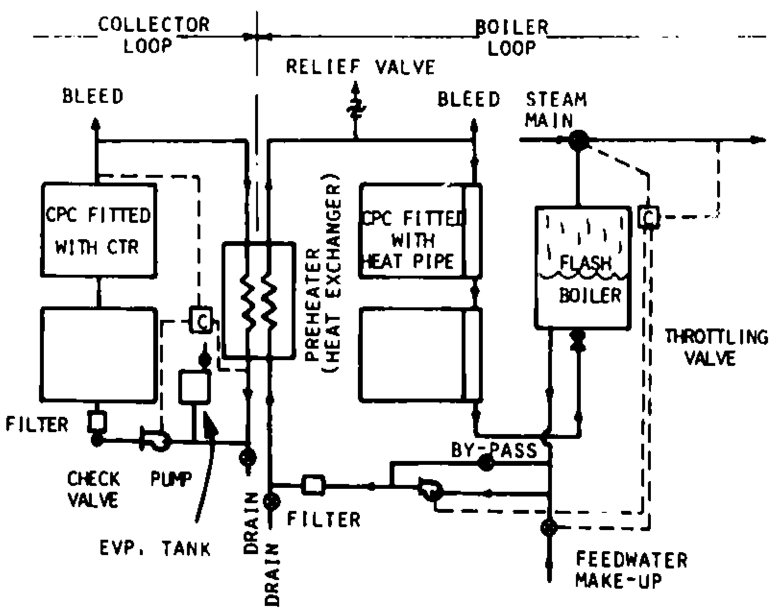

FIGURE 12. DIAGRAM OF A SYSTEM USING CPC COLLECTORS TO PRODUCE PROCESS STEAM

steam upward for delivery, while the saturated liquid is flowing downward and is circulated to the preheater and boiler for recycling. Feed water is also provided to the pump inlet to make up the fraction of the circulated water that is flashed into steam. A continuous steam generation is thus made possible. The diagram also illustrates numerous valves, tanks, filters and controls which are necessary for a satisfactory operation of the system.

1. Performance of Collectors in the Collector Loop

The CPC collector chosen for analysis in the present project is a prototype 1.5X collector designed and built by the Argonne National Laboratory. The collector is a ten trough collector module consisting of two banks in parallel with each bank made up of five troughs in series, see a schematic diagram shown in Figure 13(a). The tubular absorber used for collecting heat is designed by the General Electric, which has been illustrated in Figure 2. Input data relevant to the collector analysis are summarized in Table 3.

The computer program used for performance analysis is given in Appendix A. The program was designed to calculate temperatures (T_a, T_e, T_r and T_o) separately for each CPC trough. Since these troughs are connected in series, the exit temperature from one trough was used as the inlet temperature for the second trough. In calculating the loss coefficients, these T_a, T_e and T_r values were averaged for five troughs in each collector module, and these mean temperatures were used to calculate all the performance parameters of interest in this study. These computations were repeated for the collectors in the array. Hence, a computer run was able to generate a large body of data sufficient for performance analysis and sizing systems. Computer results are presented below.

Figure 14 shows various temperatures for each collector (module). The

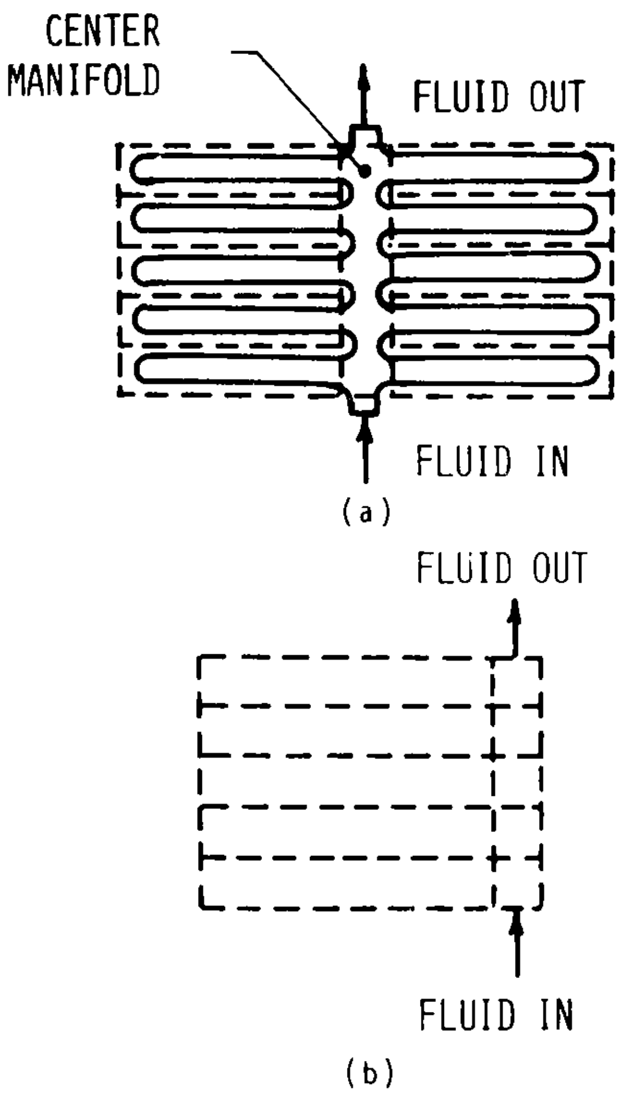

FIGURE 13. A SCHEMATIC DIAGRAM SHOWING TROUGHS LAY-OUT IN A CPC COLLECTOR FITTED WITH CTR TUBES AND A CPC COLLECTOR FITTED WITH HEAT PIPES

Table 3. Input Data for Performance Tests of Collectors in the Collector Loop

Collector Specifications (refer to Figures 2 and 3 for notations):

See Figure 13(a) for troughs lay-out.

$W = 0.1128$ m

$L = 1.1271$ m

$r_e = 0.0264$ m

$r_{r,i} = 0.0211$ m

$r_{r,o} = 0.0222$ m

$r_i = 0.0030$ m

$\text{Gap} = \text{clearance} + r_e - r_{r,o} = 0.0050 + 0.0264 - 0.0222 = 0.0092$ m

Solar Radiation Data:

$H_b(i) = 966$ W/m^2

$H_d = 100$ W/m^2

Ambient Conditions:

$T_b = 20°C$

$T_i = 25°C$

$V = 5$ m/s

Material Properties:

$\alpha_a(i) = \bar{\alpha}_a = 0.05$

$\bar{\rho}_a = 0.05$

$\tau_a(i) = \bar{\tau}_a = 0.9$

$\alpha_e(j) = \bar{\alpha}_e = 0.05$

$\bar{\rho}_e = 0.05$

Table 3. (continued)

$\tau_e(j) = \bar{\tau}_e = 0.9$

$\alpha_r(k) = \bar{\alpha}_r = 0.85$

$\bar{\rho}_r = 0.15$

$\rho_m = 0.85$

$\bar{n} = 0.6$

$\varepsilon_a = 0.85$

$\varepsilon_e = 0.85$

$\varepsilon_r = 0.05$

$k_g = 0.779$ W/m °C

Data for Heat Exchanging Media:

$$\left.\begin{aligned} k_f &= 0.28 \text{ W/m°C} \\ \dot{m}_c &= 0.0162 \text{ kg/s} \\ c_{pc} &= 3224 \text{ J/kg°C} \end{aligned}\right\} \text{(80\% Ethylene Glycol)}$$

$$\left.\begin{aligned} \dot{m}_b &= 0.017 \text{ kg/s} \\ c_{pb} &= 4170 \text{ J/kg°C} \end{aligned}\right\} \text{(Water)}$$

Heat Exchanger (Preheater) Data:

$(UA)_x = 50$ W/°C

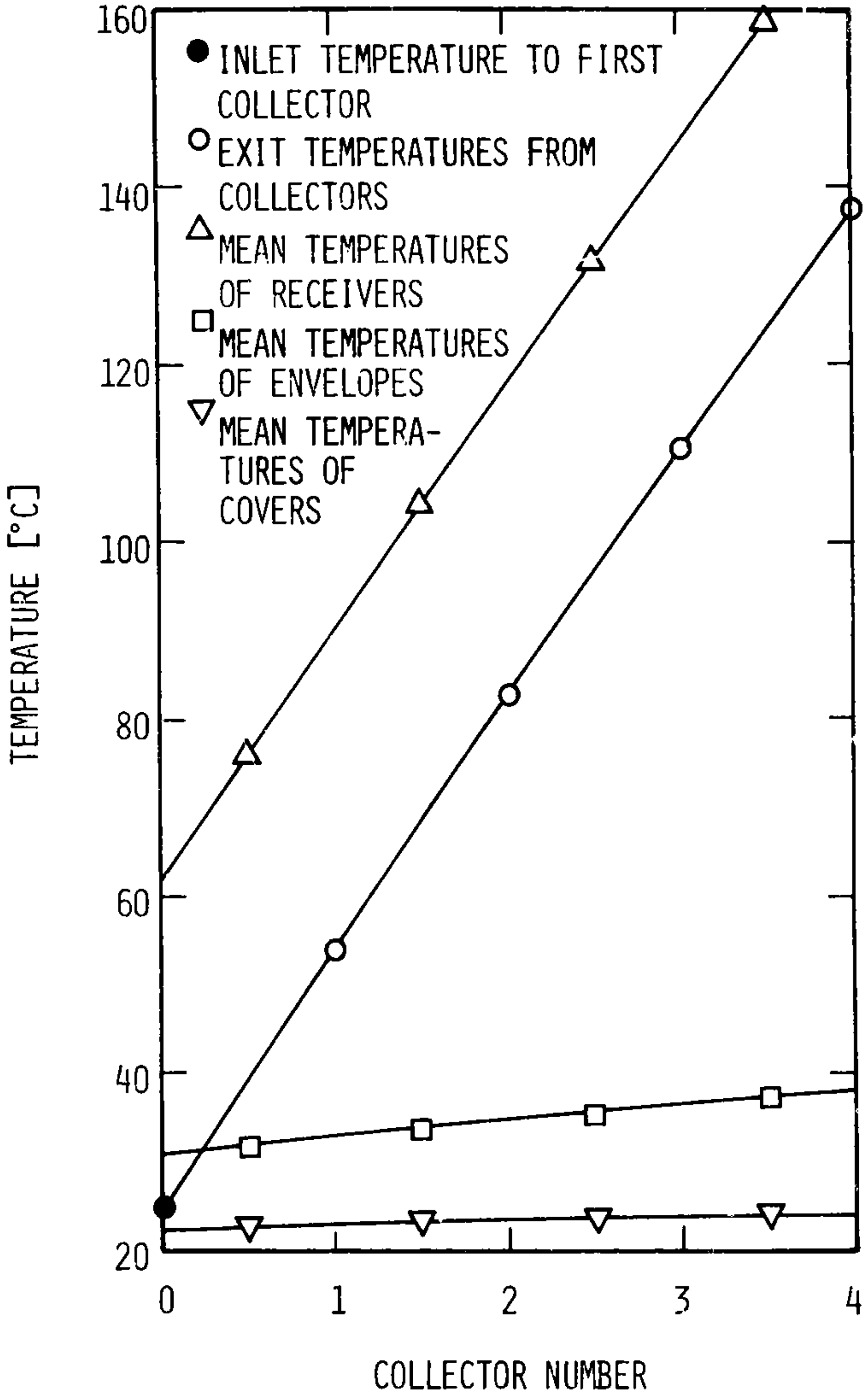

FIGURE 14. TEMPERATURE DISTRIBUTION IN A CPC COLLECTOR

The exit temperature rise in the array appears to be nearly linear. The receiver jacket, envelope and cover temperatures given in the figure are mean values for each collector; these data are therefore plotted at the mid-point for each unit. The change in the envelope temperatures is very small. As a result, the difference between the receiver and the envelope temperatures is large, signifying that the receiver loss is insignificant.

This point can be further substantiated by examining Figures 15 and 16. Here the heat loss factors (UA products) are plotted against $\Delta\bar{T}$ for the surfaces in heat transfer. The $(U_{r/e}A_r)$ value is very small in Figure 15, indicating that the receiver is well insulated by the vacuum jacket. It is also seen in these figures that the heat losses increase with both $\Delta\bar{T}$ and $\bar{T}$ (values of $\bar{T}$ have been identified near symbols). While the latter trend is expected, the former is a result of the rate of temperature rise in Figure 14. There is a reverse of trend, however, for the $U_{a/b}A_a$ curve in Figure 16. This can be ascribed to the way the $U_{a/b}$ is defined in Equation (37), where the fourth power temperatures in the numerator are in absolute units while those in the denominator are not. Hence, a small rise in T_a tends to have little effect on the quantity in the numerator while that in the denominator rises steadily with T_a. This results in a steady decline of $U_{a/b}$ as shown in Figure 16.

Both the receiver surface and the overall loss coefficients increase with $\bar{T}_r$ as shown in Figure 17. The ratio of these coefficients gives the value of F' as plotted in Figure 18. Both F' and F_R in this figure decrease as the mean receiver temperature is increased. It is noted that the abscissa in this figure is again plotted as the collector number with the mean receiver temperatures identified for each collector near the data points. The trend of these curves is primarily a result of the rate of increase of U_L with temperatures.

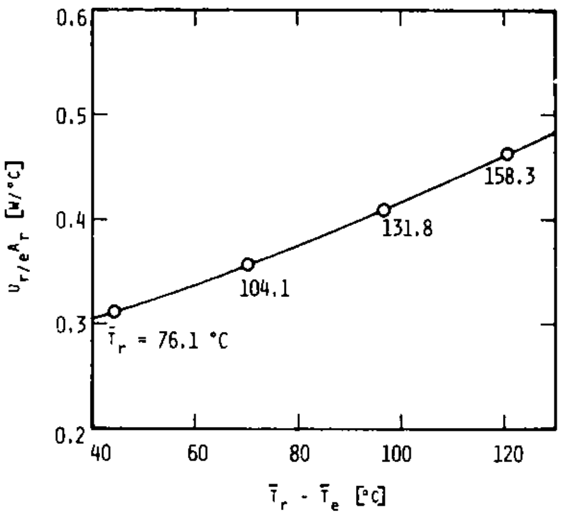

FIGURE 15. $(U_{r/e}A_r)$ VERSUS $(\bar{T}_r - \bar{T}_e)$ CURVE FOR CPC COLLECTORS

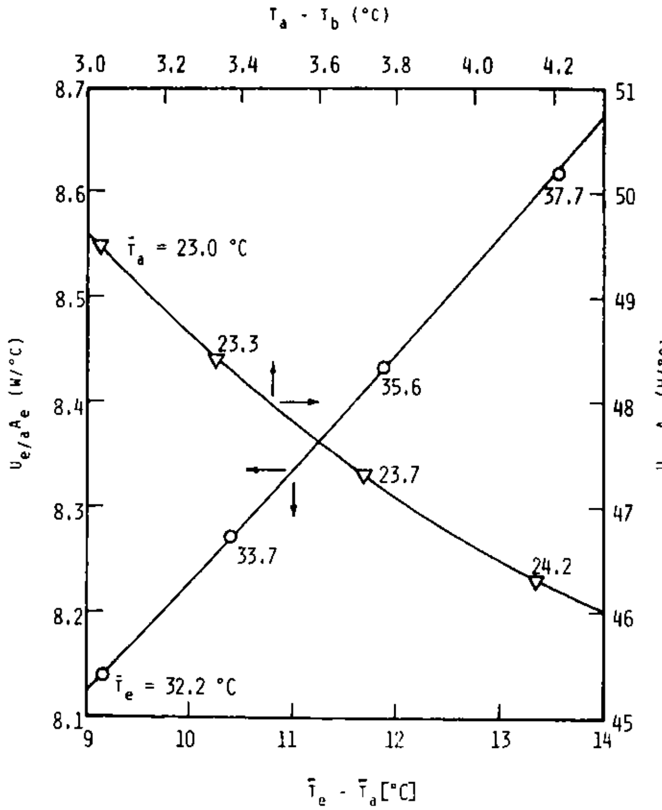

FIGURE 16. $(U_{e/a}A_e)$ AND $(U_{a/b}A_a)$ VERSUS $(\bar{T}_e - \bar{T}_a)$ CURVES FOR CPC COLLECTORS

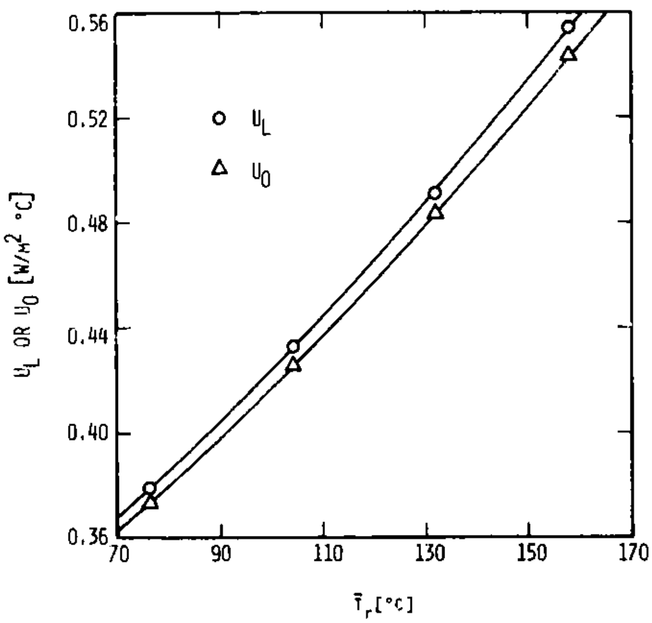

FIGURE 17. U_L AND U_0 VERSUS $\bar{T}_r$ CURVES FOR CPC COLLECTORS

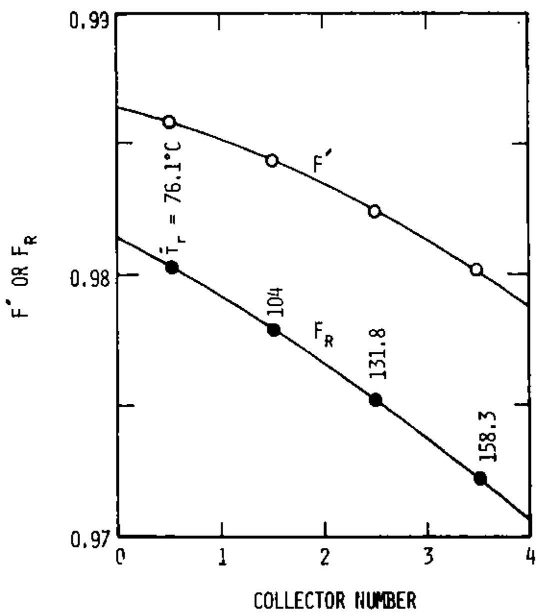

FIGURE 18. F' AND F_R CURVES FOR A SERIES OF CPC COLLECTORS

The heat exchanger penalty factor was also computed and plotted for each collector shown in Figure 19. The drop of F_x is a result of U_L which values have been identified near the data points. The F_x data in Figure 19 can be used to construct Figure 20 where Q_u has been calculated for each collector using Equation (19). $Q_{u_{ph}}$ represents the useful heat in the preheater and was obtained by multiplying the Q_u just calculated by F_x. The decline of Q_u with $\bar{T}_r$ is a result of the increased heat loss when the fluid temperature is raised.

The data given in Figure 21 provides an estimation of total useful heat if several collectors are connected in series. Again two curves are given, one represents the useful heat in the collector (ΣQ_u), the other useful heat in the preheater $\left(\Sigma Q_{u_{ph}}\right)$. Because of the large scale used for plotting the Q_u axis, the difference in Q_u values appears to be deceptively small.

Finally, the collector efficiency can be computed and plotted as shown in Figure 22. Here η and η_{ph} designate the efficiencies based on the collector circulating fluid and the heated water in the preheater, respectively. The salient point with these two curves is the weak dependency of η on T, indicating that a CPC collector is particularly attractive in high temperature applications.

It was discussed in the preceding section that the numerical value of the efficiency was dependent on which efficiency equation was used in the prediction. Computer data substantiate this observation. A plot of the efficiencies based on Equations (39), (40), (41), (42) and (45) is shown in Figure 22 (using the right expanded scale). As expected, Equation (45) gives the highest prediction. This is followed by Equation (42). Equations (39), (40) and (41) give the lowest values. The reason for this has been explained previously (see the text following Equation (45)).

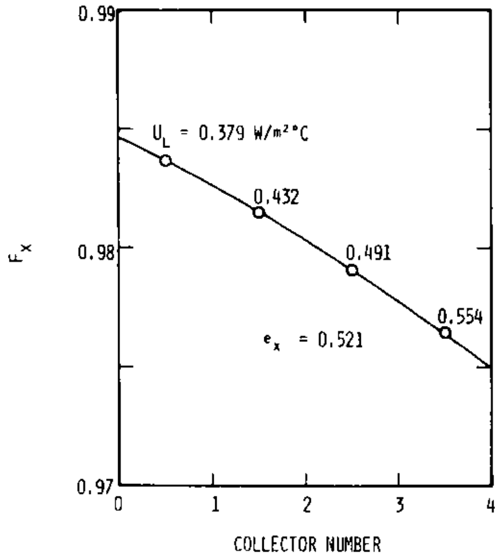

FIGURE 19. HEAT EXCHANGER PENALTY FACTOR FOR A CPC COLLECTOR

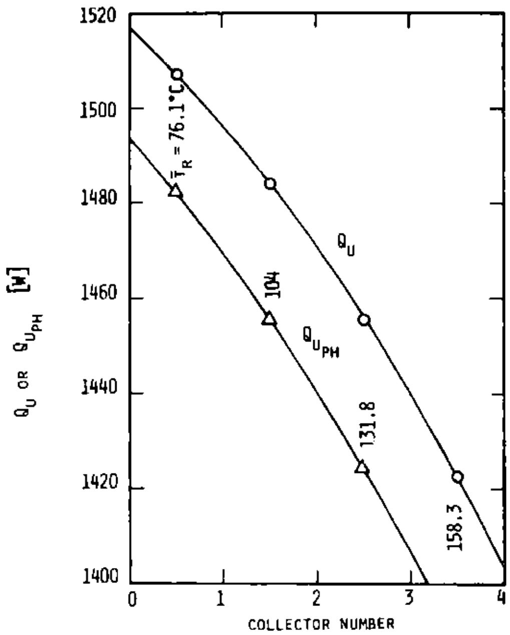

FIGURE 20. USEFUL HEAT GAINS IN A SERIES OF CPC COLLECTORS

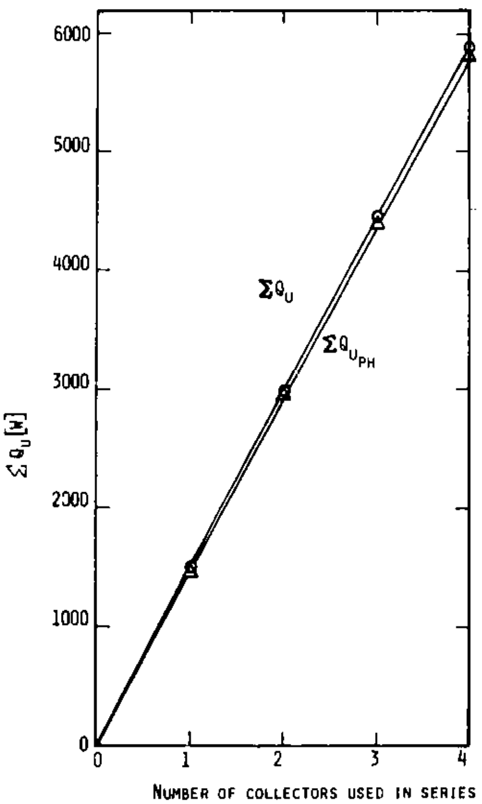

FIGURE 21. TOTAL USEFUL HEAT IN A SERIES OF CPC COLLECTORS

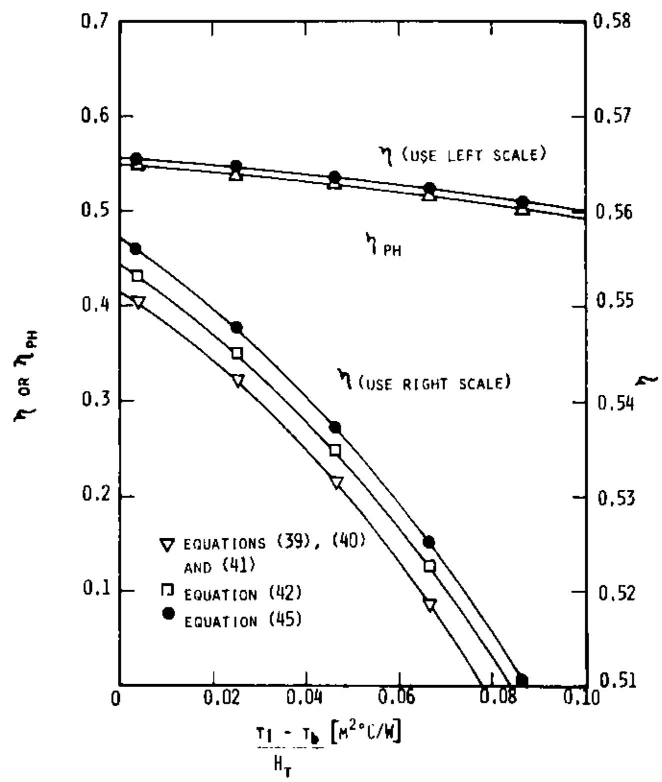

FIGURE 22. EFFICIENCY CURVES FOR A CPC COLLECTOR

The analysis presented in this subsection was validated by using experimental data as shown in Figure 23. Water was taken as the collector circulation fluid because of the availability of its test data. The prediction appears to be in good agreement with experiments.

2. Boiler Loop Analysis

The CPC collectors in the boiler loop employ heat pipes to transmit heat. These pipes were designed based on the analysis given in the preceding section. Property values used in the design are summarized in Table 4. A detailed heat pipe analysis yields a set of specifications as shown in Table 5. In order to characterize the heat pipe performance some design parameters were also computed and listed in Table 6. For the CPC collectors chosen to use in the boiler loop, the maximum heat load to be carried by each heat pipe is 164 W. The heat loads at capillary, sonic, entrainment and boiling limitations are found to be 389, 84027, 2635 and 406 W, respectively. They are far greater than needed; a safe operation of the pipe can be assured.

In order to evaluate the performance of collectors in the boiler loop, it is necessary to determine the heat transfer characteristics of heat pipes. This was done by using Equations (68) to (75), and the results are listed in Table 7. The major resistance to heat flow appears in the wick, which is typical for a heat pipe. The overall conductance based on the cross-sectional area of the pipe is calculated to be about 25 times that of a solid copper bar of the same cross section and length. The reason to use heat pipes to transmit heat is thus obvious.

The computer program previously used for collector loop analysis was modified to use in the boiler loop. There is a minor simplification in the new program. Since the water at the condenser section was treated as flow

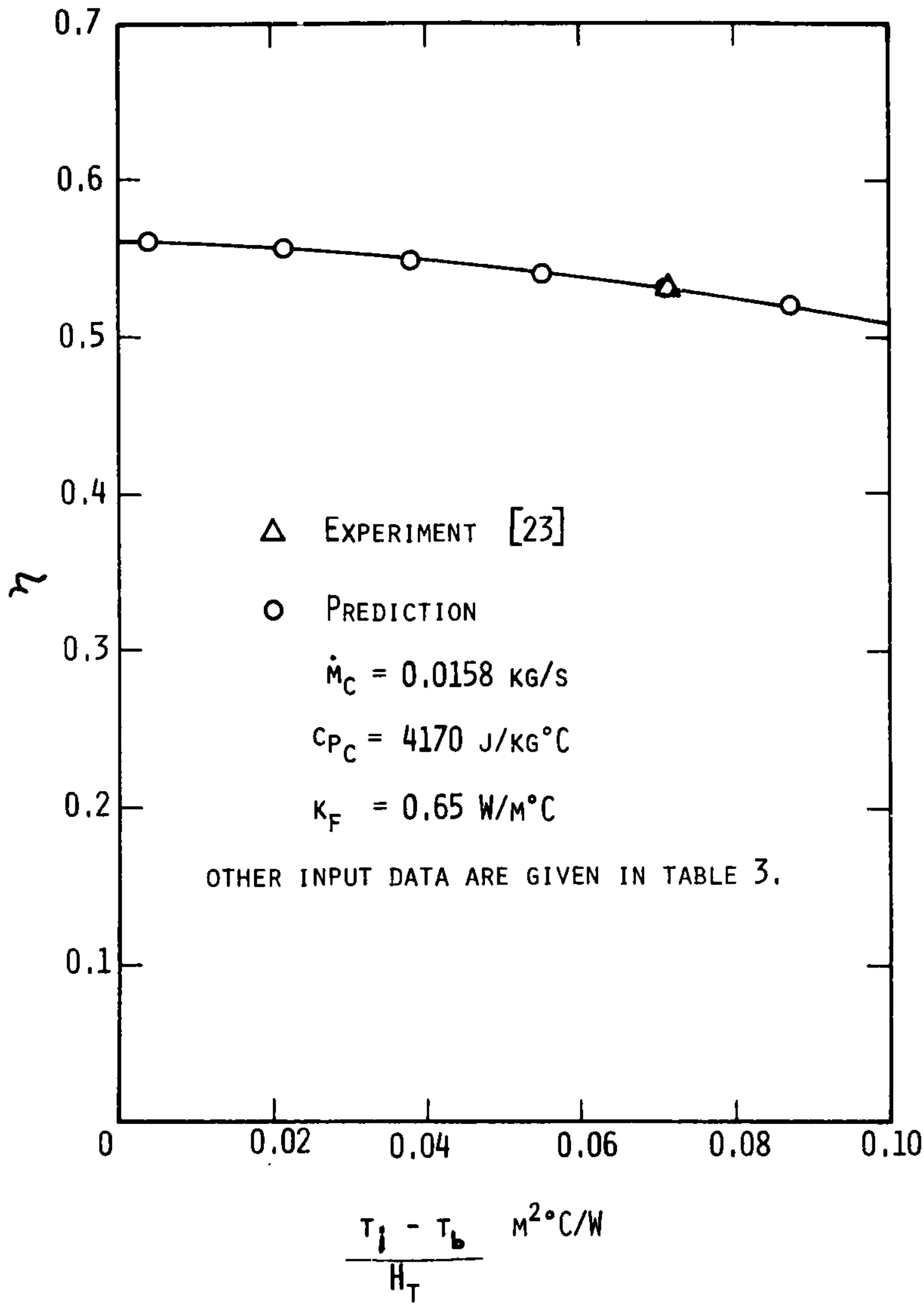

FIGURE 23. VALIDATION OF ANALYSIS USING TEST DATA

Table 4. Properties of Heat Pipe Materials at 160°C

Container and Cap - Copper

$k_p = 372$ W/m°C

$s_u = 1.38 \times 10^8$ N/m^2

Working Fluid - Water

$p_v = 6.81 \times 10^5$ N/m^2

$h_{fg} = 2074$ kj/kg

$\gamma_v = 1.33$

$\xi = 4.66 \times 10^{-2}$ N/m

$\rho_1 = 909$ kg/m^3

$\rho_v = 3.27$ kg/m^3

$\mu_1 = 0.17$ cp

$\mu_v = 1.49 \times 10^{-2}$ cp

$k_1 = 0.679$ W/m°C

Table 5. Heat Pipe Specifications

Pipe Container Material:	Copper
Working Fluid:	Water
Vapor, Temperature and Pressure:	Self adjustable according to operating conditions

Pipe Specifications:

Elevation (end-to-end, condenser higher) - 0.0254 m

Evaporator Length - 1.2192 m

Adiabatic Section Length - 0.1016 m

Condenser Length - 0.1524 m

Pipe Dimensions - BWG 20

0.01905 m OD

0.01727 m ID

End Cap Thickness - 0.0008128 m (flat cap)

Wick Specifications:

Wick Thickness - 0.004572 m

Wire-screen Mesh

Mesh Number = 50

Wire Diameter = 0.000254 m

Wick Material = Copper

Table 6. Heat Pipe Design Details

Maximum Heat Load to be Carried by Each Heat Pipe $= (H_b(i) + H_d)\ 2WL_e\eta_o$

$= 164$ W

Parameters Relating to Fluid Selection:

(Fluid - Water) $N_l = 5.17 \times 10^{11} W/m^2$

$N_{k_l} = 3.51 \times 10^{11} W^2/m^3{}^\circ C$

Parameters Relating to Container Selection:

(Container - Copper) $N_{k_p} = 4.17 \times 10^{10}$ J kg/sec^{3}m^2°C

Wick Data: $\phi = 0.5877$

$K = 6.31 \times 10^{-10}\ m^2$

$r_c = 0.3937$ m

Friction Coefficients: $F_l = 0.783$ N sec/Jm^3

$F_v = 0.658$ N sec/Jm^3

Operating Limitations: $Q_{max,\ capillary} = 389$ W

$Q_{max,\ sonic} = 84{,}027$ W

$Q_{max,\ entrainment} = 2{,}635$ W

$Q_{max,\ boiling} = 406$ W

Comments: All $Q_{max} > 164$ W, safe operation is assured.

Check Reynolds and Mach Numbers for Vapor Flow:

$R_e = 831\ (<2{,}300)$

$M = 9 \times 10^{-4} (<0.2)$

Table 7. Summary of Heat Transfer Characteristics of the Designed Heat Pipe

$R_{p,e} = 9.28 \times 10^{-9}\ m^2 °C/W$

$R_{w,e} = 1.21 \times 10^{-5}\ m^2 °C/W$

$R_v = 1.62 \times 10^{-9}\ m^2 °C/W$

$R_{w,c} = 9.67 \times 10^{-5}\ m^2 °C/W$

$R_{p,c} = 7.44 \times 10^{-8}\ m^2 °C/W$

$U_p = 9.18 \times 10^{3}\ W/m^2 °C$

in an annulus, and the convective coefficient of water has been incorporated into the overall heat transfer coefficient from the receiver surface to water (discussed previously in Section II, 3), a separate evaluation of the heat exchanger penalty is no longer needed. This new computer program has been included as Appendix B to this report. A sample run was also made using the data given in Table 8 as inputs.

An examination of the data output reveals that the trends of data are quite similar to the ones seen in Figures 14 to 18. There is one exception - the collector efficiency in the boiler loop is about 25% lower than before. This can be ascribed to the fact that the gap loss for these boiler collectors is much higher. Using data given in Tables 3 and 8, it is easy to show that, for the collectors in the collector loop, $p = 0.933$, whereas those in the boiler loop, $p = 0.782$. The gap loss is thus important to the collector performance. The computer data for boiler collectors have been given in the appendix following the computer program, a separate data plot is not attempted.

The analysis made above provides a means of evaluating the performance of the total system. Use is made of the equivalent thermodynamic circuit shown in Figure 24. Here the collectors in both collector and boiler loops are represented by a blackbox and $\left(Q_{u_{ph}} + Q_{u_b}\right)$ is used to denote the constant-pressure heat input to the boiler water. Process 2-3 represents a throttling process. This process enables a portion of the subcooled (or saturated) liquid at elevated pressures and temperatures to flash into steam. The flash boiler behaves much like a separator to direct the saturated steam upward to point 5 while the saturated water at lower pressures settles down and discharges at point 4. The portion of the water that is flashed into steam is replenished by the makeup feedwater which mixes with the water at state 4

Table 8. Input Data for Performance Tests of Collectors in the Boiler Loop

Collector Specifications (refer to Figures 2 and 11 for notations):

See Figure 13 (b) for troughs lay-out.

$W = 0.1128$ m

$L = 1.2192$ m (Corresponds to heat pipe evaporator length)

$r_e = 0.0174$ m

$r_{p,o} = 0.0095$ m

$r_a = 0.0127$ m

$L_e/L_c = 8$

Gap = Clearance + $r_e - r_{p,o} = 0.0050 + 0.0174 - 0.0095 = 0.0129$ m

Solar Radiation Data:

$H_b(i) = 966$ W/m^2

$H_d = 100$ W/m^2

Ambient Conditions:

$T_b = 20°C$

$T_i = 137.39°C$ (Assume four collectors in series in the collector loop)

$V = 5$ m/s

Material Properties:

$\alpha_a(i) = \bar{\alpha}_a = 0.05$

$\bar{\rho}_a = 0.05$

$\tau_a(i) = \bar{\tau}_a = 0.9$

$\alpha_e(j) = \bar{\alpha}_e = 0.05$

$\bar{\rho}_e = 0.05$

Table 8 (Continued)

$\tau_e(j) = \bar{\tau}_e = 0.9$

$\alpha_r(k) = \bar{\alpha}_r = 0.85$

$\bar{\rho}_r = 0.15$

$\rho_m = 0.85$

$\bar{n} = 0.6$

$\varepsilon_a = 0.85$

$\varepsilon_e = 0.85$

$\varepsilon_r = 0.05$

<u>Data for Water in the Boiler Loop:</u>

$k_f = 0.65$ W/m°C

$\dot{m}_b = 0.017$ kg/s

$c_{p_b} = 4170$ J/kg°C

<u>Heat Pipe Data:</u>

$U_p = 9180$ W/m^2°C

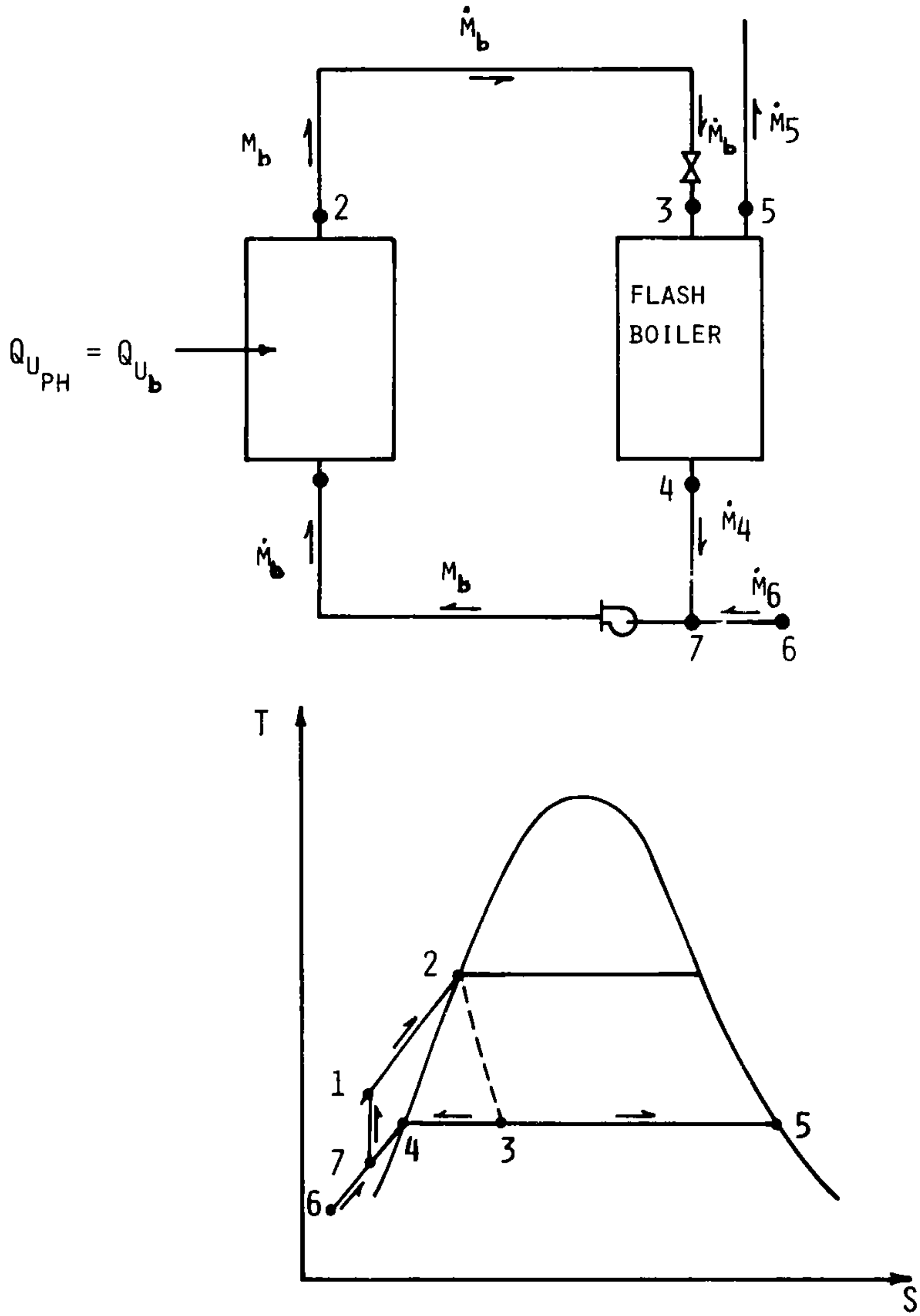

FIGURE 24. THERMODYNAMIC CIRCUIT AND T-S DIAGRAMS

to form state 7. The pumping process can be modeled as isentropic and is used to pressurize water in the boiler loop. The total thermodynamic cycle can be plotted using a temperature-entropy diagram and shown in the lower half of the figure. A thermodynamic analysis follows below.

It is easy to show by using the continuity equation that

$$\dot{m}_5 = \dot{m}_6 \tag{78}$$

By using the first law of thermodynamics, it can be derived that the quality of steam at point 3 is

$$x_3 = \frac{h_3 - h_4}{h_5 - h_4} \tag{79}$$

where h's are enthalpies.

Using the same law, the system at the T-joint at pump inlet can be analyzed as follows:

$$h_7 = (1 - x_3)\, h_4 + x_3 h_6 \tag{80}$$

Similarly for the pump itself,

$$h_1 = h_7 + v_7\, (p_1 - p_7) \tag{81}$$

where v is the specific volume. Equations (78) to (81) can be used together to predict the steam flow rate.

For illustration purposes, a sample calculation is provided below. It is assumed that

$$p_3 = p_4 = p_5 = p_6 = p_7 = 1 \text{ atm}$$

$$T_6 = 20°\text{C}$$

$$p_2 = 3.08 \text{ X } 10^5 \text{ N/m}^2 \doteq 3 \text{ atm}$$

and point 2 is a saturated liquid. The analysis given above can be used to predict

$$\begin{aligned} x_3 &= 6.5\% \\ h_1 &= 4 \text{ X } 10^5 \text{ J/kg} \\ h_7 &= 3.98 \text{ X } 10^5 \text{ J/kg} \end{aligned} \tag{82}$$

and

$$Q_{ph} + Q_b = (h_2 - h_1)\ \dot{m}_b$$
$$= 1.644 \times 10^5 \times \dot{m}_b \text{ W} \tag{83}$$

Since $\dot{m}_b$ has been chosen to be 0.017 kg/s in the computer simulation (see Table 8)

$$Q_{ph} + Q_b = 2.79 \times 10^3 \text{ W} \tag{84}$$

which represents the total heat input needed for the circulating water.

There are several ways by which this heat demand can be met, see Figure 25. If there is no collector in the collector loop, it takes about 4.5 boilers to supply this amount of heat. If there is one collector in the collector loop, then 2.1 boilers must be used. Of course, if two collectors are available in the collector loop, then these collectors will be sufficient to meet the need. In practice, the boiler numbers cited here will be rounded upward to account for system heat losses. Figure 25 is seen to be an excellent tool for design purposes.

The analysis given above also provides a means for predicting the amount of steam generation. Since $\dot{m}_6$ has been chosen as 0.017 kg/s in the computer simulation, the amount of steam generation can readily be calculated as

$$\dot{m}_5 = 0.065 \times 0.017 = 1.1 \text{ g/s}$$

where 0.065 on the right of the equation comes from Equation (82).

This steam generation rate can be checked by considering the entire boiler loop as a system, which is identified by its system boundary shown in Figure 26. For this system the interactions between the system and the surroundings include the heat transfer $(Q_{ph} + Q_b)$, the shaft work to drive the pump, i.e.

$$w = h_1 - h_7$$

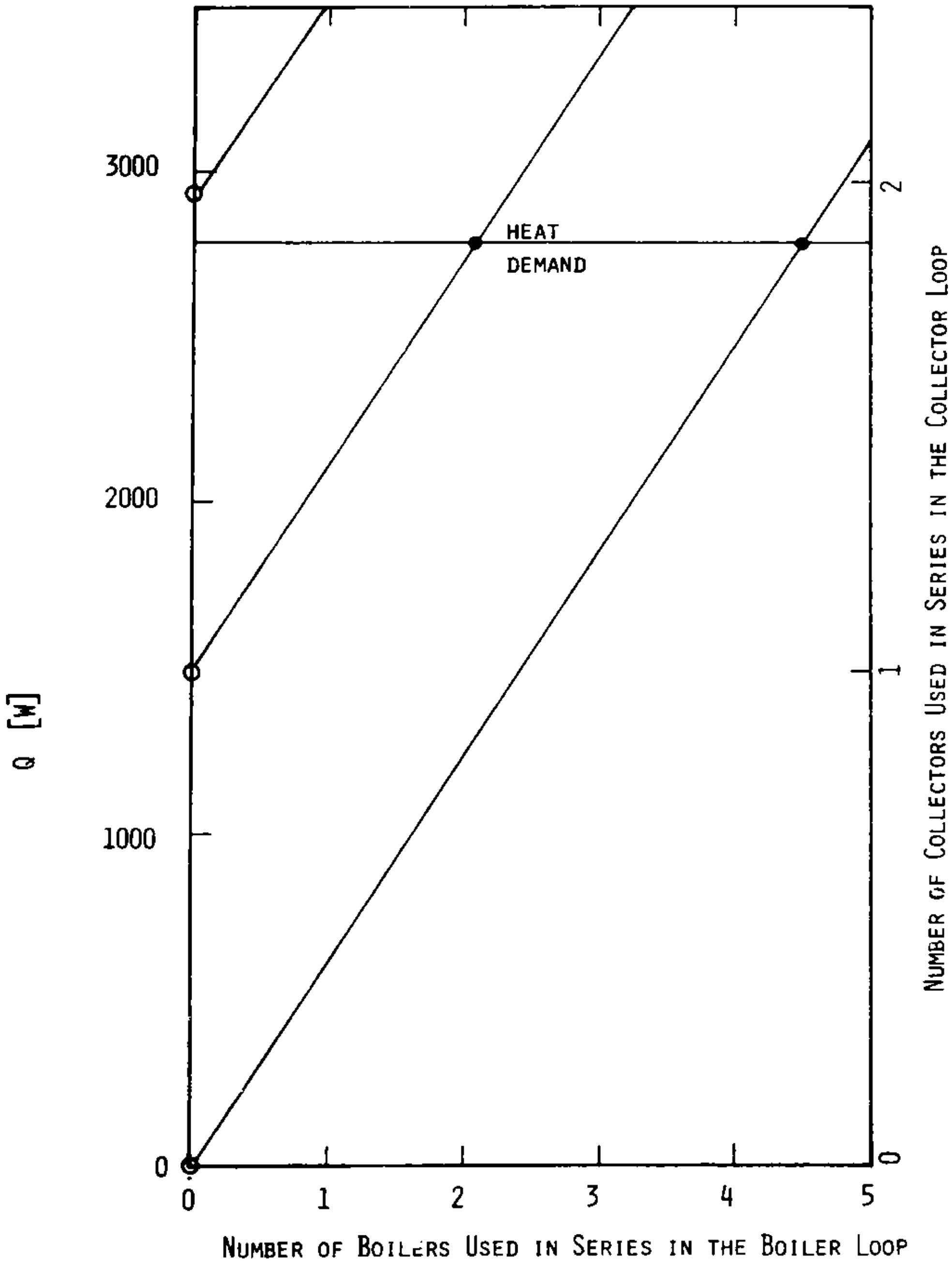

Figure 25. A Design Chart for Steam Generation

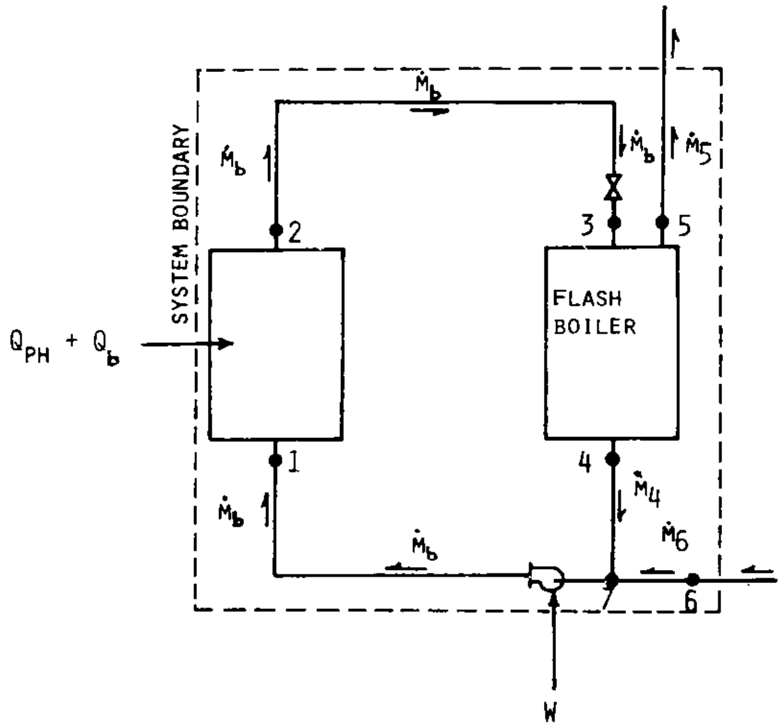

Figure 26. A Simplified System Analysis

and fluid flowing in and out of the system. According to the previous analysis the total energy (heat and work) input to the system is

$$Q_{total} = 2790 + 0.02 \times 10^5 \times 0.017 = 2824 \text{ W}$$

This value is in close agreement with the energy required to convert 1.1 g/s of water at 20°C to steam at 100°C, which is 2847 W.* The error of 0.8% can be ascribed to the fact that the specific heat of water has been treated as a constant in the simple analysis (see footnote). The numerical error also contributes to the difference.

3. Discussion

It should be noted that in the present design, the system uses a double-loop circuit for energy collection. As has been shown, a total heat input is all that is needed to convert the feed water to steam. As such, the use of double-loop appears to be unnecessary. Indeed, if the system is designed to produce hot "water" for industrial process heat applications, the collectors in the collector loop, with ethylene glycol used as collector circulating fluid, should be adequate to provide the heat demand. It will be a different state of affairs, however, if the system is designed to produce steam. Then, various constraints should be considered. A one-step heating in the collector loop may be impossible because of the low boiling points of glycols.

---

*Energy required to raise the temperature of water from 20 to 100°C is

$$Q_{20\,-\,100°C} = 1.1 \times 4.7 \times (100 - 20) = 367 \text{ W}$$

To convert this water to steam requires

$$Q_{100°C \text{ water} - 100°C \text{ steam}} = 1.1 \times 2254.6 = 2480 \text{ W}$$

As a point of further interest, the use of the present system for supplying hot water in the industrial process heat applications is also analyzed as shown in Figure 27. Here the figure was constructed on the basis of two collectors in series and the family of curves is parameterized by the water inlet temperature. As is totally expected, an increase of the water flow rate as well as a lowering of the water inlet temperature depresses the water exit temperature.

The heat pipes inside the boiler loop collectors use water as a working fluid. Water is known to have a high freezing point, which makes the collector susceptible to freeze damage at low temperatures. It should be noted that the decision of using water as a working fluid in heat pipes is solely dictated by its high liquid transport number [Equation (48)]. Many organic liquids are available and have low freezing points, but they are inferior to water in this respect. There are various factors to be weighed in selecting a working fluid [3-5]. Research on heat pipes for moderate temperature applications is still active presently.*

The analysis given in this report was made based on a negligible heat loss from pipes and accessories. In practice, such a parasatic loss is unavoidable and these losses should be taken into consideration in the final design. On the other hand, in the boiler loop the collectors were analyzed based on a water inlet temperature of 137.39°C. This temperature was taken based on the assumption that there were four collectors in series in the collector loop. (The resulting preheater exit temperature is of this magnitude). Calculations

---

*Philco Italiana uses EHS 112 as a working fluid in their heat-pipe solar collectors. North American Philips Lighting has just developed a heat-pipe receiver tube using isobutane as a working fluid.

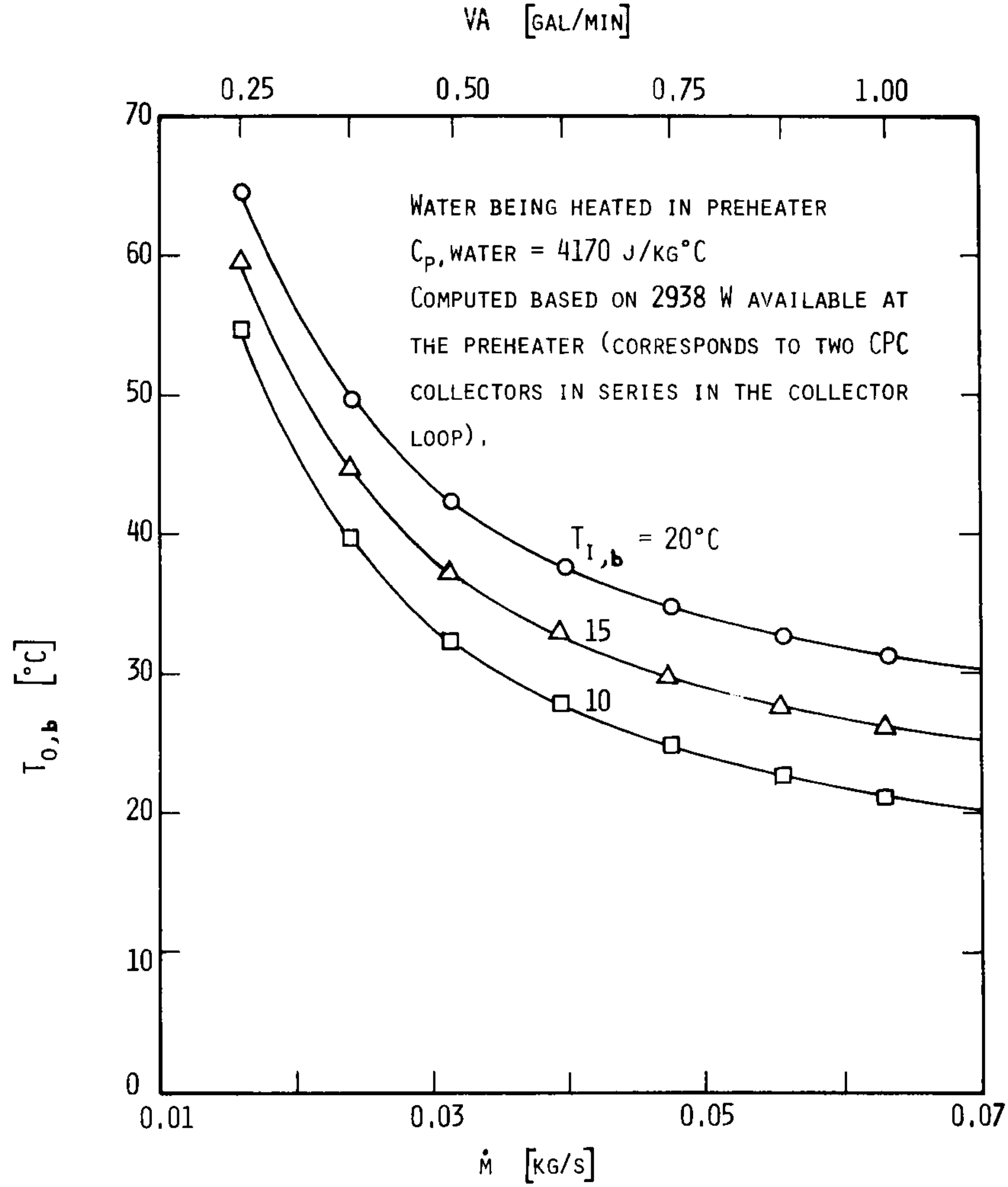

FIGURE 27. EXIT WATER TEMPERATURE PREDICTION CHART

based on this inlet temperature are expected to yield a slightly higher heat loss. Hence, the actual heat gains are expected to be slightly higher than those given in Figure 25. The difference is, nevertheless, small for the small $U_{r/e}$ occurring in CPC collectors.

Finally, it is noted that, in the installation of collectors in the boiler loop, these collectors are rotated in the sense that the condenser section is slightly higher than the evaporator. The number of collection hours for a rotated CPC collector has been analyzed and reported in [21]. Tilt angle adjustments can be computed accordingly with the help of this reference.

IV. CONCLUSIONS

Based on the study made in this report some conclusions can be drawn and given as follows:

1. It has been shown that the proposed system can be used to produce low quality steam for industrial process heat purposes. The system consists of two series of collectors divided into two loops. The collectors in the collector loop use ethylene glycol for collector circulation fluid which is known for its low freezing point and high boiling point. The collectors in the boiler loop use heat pipes for transmitting heat. These heat pipes enable heating to take place outside its condenser section. The circulating water in the boiler loop is slightly pressurized to raise its boiling point. It is expected that, with these special designs, problems associated with weak receiver tube, scaling and plumbing problems can all be resolved in steam generation.

2. The CPC collectors have shown to be an excellent collector for industrial process heat applications. Not only is its simplicity in design, requiring only occasional adjustments of tilt angles to intercept solar energy, but also is the fact that the CPC collector has an efficiency curve that is very weakly dependent on the receiver temperatures. The CPC collector is thus superior to a constant tracking trough or dish collector and is particularly attractive in high temperature applications.

3. The computer simulations given in this report have shown that the proposed system is technically feasible. Thermodynamic analyses given here also verify the validity of the analysis. The computer program, as well as the detailed analyses presented in this report, will be helpful to the prediction of thermal processes in a CPC collector and will be instrumental to the future system analysis.

V. REFERENCES

1. Information Source: SERI
2. Welford, W. T., and Winston, R., The Optics of Nonimaging Concentrators, Academic Press, 1978.
3. Winter, E. R. F., and Barsch, W. O., The Heat Pipe, Advances in Heat Transfer 7 (Editors: T. F. Irvine, Jr., and J. P. Hartnett), Academic Press, 1971.
4. Chi, S. W., Heat Pipe Theory and Practice: A Source Book, Hemisphere Publishing, 1976.
5. Dunn, P., and Reay, D. A., Heat Pipes, Pergamon Press, 1975.
6. Rabl, A., Optical and Thermal Properties of Compound Parabolic Concentrators, Solar Energy, Vol. 18, 497, 1976.
7. Kreider, J. F., Performance Study of the Compound Parabolic Concentrator Solar Collector, Environmental Consulting Services, Inc., Boulder, Colorado, 1974.
8. Kreider, J. F., Thermal Performance of the Compound Parabolic Concentrator Solar Collector - Phase II, Environmental Consulting Services, Inc., Boulder, Colorado, 1975.
9. Winston, R., Principles of Solar Concentrators of a Novel Design, Solar Energy, Vol. 16, 89, 1974.
10. Rabl, A., Radiation Transfer through Specular Passages - A Simple Approximation, International Journal of Heat and Mass Transfer, Vol. 20, 323, 1977.
11. Rabl, A., Comparison of Solar Concentrators, Solar Energy, Vol. 18, 93, 1975.

12. Goodman, N. B., Rabl, A., and Winston, R., Optical and Thermal Design Considerations for Ideal Light Collectors, Sharing the Sun, Vol. 2, 336, 1976.

13. Whiller, A., Design Factors Influencing Solar Collectors, Low Temperature Engineering Applications of Solar Energy, ASHRAE, 1967.

14. McAdams, W. C., Heat Transmission, Third Edition, McGraw-Hill, 1954.

15. Kays, W. M., Convective Heat and Mass Transfer, McGraw-Hill, 1966.

16. Hottel, H. C., and Woertz, B. B., Performance of Flat-plate Solar-Heat Collectors, Transactions of ASME, Vol. 64, 91, 1942.

17. Hottel, H. C., and Whillier, A., Evaluation of Flat-plate Collector Performance, Transactions of the Conference on the Use of Solar Energy, Vol. 2, Part 1, 74, 1958.

18. Bliss, R. W., The Derivations of Several Plate Efficiency Factors Useful in the Design of Flat-plate Solar-Heat Collectors, Vol. 3, 55, 1959.

19. deWinter, F., Heat Exchanger Penalties in Double Loop Solar Water Heating Systems, Solar Energy, Vol. 17, 335, 1975.

20. Lundberg, R. E., McCuen, P. A., and Reynolds, W. C., Heat Transfer in Annular Passages. Hydraudynamically Developed Laminar Flow with Arbitrarily Prescribed Wall Temperature or Heat Flux, International Journal of Heat and Mass Transfer, Vol. 6, 495, 1963.

21. Miller, C. W., Collection Times for Trough-Type Concentrators Having Arbitrai rientation, Solar Energy, Vol. 20, 399, 1978.

22. Information Source: Union Carbide

23. Ar nne National Laboratory Solar Energy Program Annual Report, ANL-79-16.

APPENDIX A. A COMPUTER PROGRAM TO ANALYZE THERMAL PROCESSES IN A SERIES OF CPC COLLECTORS FITTED WITH CTR TUBES

The computer program given in this appendix is designed to generate a large body of data relevant to the thermal processes in a CPC collector fitted with a CTR. A single run of the computer program yields data for an array of six collectors in series. Line number 62 can be changed if more collectors are needed. Definitions for input variables are given as follows.

RI = r_i

RO = $r_{r,o}$

RE = r_e

HW = w

WLEN = L

GAP = Clearance + $(r_e - r_{r,o})$

REFN = $\bar{n}$

TUBES = No. of troughs in parallel*

RRI = $r_{r,i}$

HBCI = $H_b(i)$

HD = H_d

TB = T_b

TI = T_i

FLOWR = $\dot{m}_c$

WIND = V

*TUBES = 2 for the collector shown in Figure 13.

ER = ε_r

EE = ε_e

EA = ε_a

CP = c_{p_c}

TKF = k_f

TKG = k_g

ARK = $\alpha_r(k)$

ARM = $\bar{\alpha}_r$

RRM = $\bar{\rho}_r$

AEJ = $\alpha_e(j)$

AEM = $\bar{\alpha}_e$

REM = $\bar{\rho}_e$

TEJ = $\tau_e(j)$

TEM = $\bar{\tau}_e$

AAI = $\alpha_a(i)$

AAM = $\bar{\alpha}_a$

RAM = $\bar{\rho}_a$

TAI = $\tau_a(i)$

TAM = $\bar{\tau}_a$

RMIR = ρ_m

EPS = Convergence criterion for iteration

PASS = No. of troughs in series*

---

*PASS = 5 for the collector shown in Figure 13.

FLOWF = $\dot{m}_b$

CPF = c_{p_b}

UA = $(UA)_x$

Definitions for output variables are given as follows:

TA = T_a or $\bar{T}_a$

TE = T_e or $\bar{T}_e$

TR = T_r or $\bar{T}_r$

TO = T_o

UOP = $U_{r/e}A_r$

UWP = $U_{e/a}A_e$

UTP = $U_{a/b}A_a$

ULP = U_LA_r

UL = U_L

UO = U_o

FPR = F'

FSR = F_R

CMIN = $(\dot{m}c_p)_{min}$

CMAX = $(\dot{m}c_p)_{max}$

TUNIT = $(UA)_x/(\dot{m}c_p)_{min}$

EHX - e_x

FHX = F_x

QUY = Q_u, Equation (28)

QUZ = Q_u, Equation (29)

QU1 = Q_u, Equation (32)

QU2 = Q_u, Equation (34)

QU3 = QU2 times F_x

QUC = $\dot{m}_c \; c_{p_c} \; (T_o - T_i)_c$

EFFY = η, Equation (39)

EFFZ = η, Equation (40)

EFF1 = η, Equation (41)

EFF2 = η, Equation (42)

EFF3 = EFF2 times F_x

EFFC = η, Equation (45)

The computer program is given on the next page.

```
REQUESTED OPTIONS: NOTERM,

OPTIONS IN EFFECT: NAME(MAIN) NOOPTIMIZE LINECOUNT(60) SIZE(MAX) AUTODBL(NONE)
                   SOURCE EBCDIC NOLIST NODECK OBJECT MAP NOFORMAT GOSTMT NOXREF NOALC NOANSF NOTERM FLAG(I)

      C      THIS PROGRAM SIMULATES THERMAL PROCESSES IN A CPC
             DIMENSION WA(10),WE(10),WR(10)
             READ (5,1) RI,RO,RE,HW,WLEN,GAP,REFN,TUBES,RRI
           1 FORMAT (9F8.4)
             READ (5,2) HBCI,HD,TB,TI,FLOWR,WIND
           2 FORMAT (6F8.4)
             READ (5,3) ER,EE,EA,CP,TKF,TKG
           3 FORMAT (6F8.4)
             READ (5,4) ARK,ARM,RRM,AEJ,AEM,REM,TEJ,TEM
           4 FORMAT (8F8.4)
             READ (5,5) AAI,AAM,RAM,TAI,TAM,RMIR
           5 FORMAT (6F8.4)
             READ (5,11) EPS,PASS,FLOWF,CPF,UA
          11 FORMAT (5F10.5)
             WRITE (6,17)
          17 FORMAT (12H INPUT DATA:///)
             WRITE (6,6) RI,RO,RE,HW,WLEN,GAP,REFN,TUBES,RRI
           6 FORMAT (9F10.4///)
             WRITE (6,7) HBCI,HD,TB,TI,FLOWR,WIND
           7 FORMAT (6F10.4///)
             WRITE (6,8) ER,EE,EA,CP,TKF,TKG
           8 FORMAT (6F10.4///)
             WRITE (6,9) ARK,ARM,RRM,AEJ,AEM,REM,TEJ,TEM
           9 FORMAT (8F10.4///)
             WRITE (6,10) AAI,AAM,RAM,TAI,TAM,RMIR
          10 FORMAT (6F10.4///)
             WRITE (6,16) EPS,PASS,FLOWF,CPF,UA
          16 FORMAT (5F10.5///)
             NPASS=PASS
             TIN=TI
             PI=3.14159
             SIGMA=5.663E-8
             DELTA=-6.
             YB=TB+273.
             AR=2.*PI*RO*WLEN
             AE=2.*PI*RE*WLEN
             AA=2.*HW*WLEN
             ARO=AR
             AEO=AE
             AAO=AA
             AROL=AR/WLEN
             P=1.-(GAP/AROL)
             RMIRE=RMIR**REFN
             HBTR=HBCI*TAI*RMIRE
             ERI=1./ER
             EEI=1./EE
             EAI=1./EA
             COEF=FLOWR*CP/TUBES/AR
             FAC=WLEN/AR
             COEG=FAC/(1./6.855/TKF+0.31831*ALOG(RO/RRI)/TKG)
             COEQ=COEF/COEG
             QDR=HBTR*TEJ*P*(ARK+ARM*RRM*REM*AR/AE)*AA/AR
             QRC=HBCI*(AAI+AAM*TAI*REM*RMIRE**2)*AA/AR
```

73

```
ISN 0054           QBE=HBTF*(AEJ+AEN*REN*RAN*EMIRE**2*AE/AA+AEN*RRN*TEJ)*AA/AR
ISN 0055           QDR=HD*TAN*TEN*ARN*EMIRE*F*(1.+RRN*REN*AR/AE)
ISN 0056           CDC=HD*AAN*(1.+TAN*REN*EMIRE**2)*AA/AR
ISN 0057           CDE=HD*TAN*EMIRE*AEN*(1.+REN*RAN*EMIRE**2*AE/AA+RRH*TEN)
ISN 0058           EPE=SIGMA/(ERI+AR*(EEI-1.)/AE)
ISN 0059           EEA=(AE/AR)*SIGMA/(EEI+AE*(EAI-1.)/AA)
ISN 0060           EAS=EA*SIGMA*AA/AR
ISN 0061           HAB=5.7+3.8*WIND
ISN 0062           CAB=HAB*AA/AR
ISN 0063           STEP=0.01
ISN 0064           DO 48 MIT=1,6
ISN 0065           WRITE (6,21) MIT
ISN 0066        21 FORMAT (1H1,30H OUTPUT DATA FOR COLLECTOR NO.I2,1H:///)
ISN 0067        22 DO 24 IT=1,NPASS
ISN 0068           J=1
ISN 0069        23 VTA=J
ISN 0070           IF (J-600) 25,25,74
ISN 0071        25 TA=TB+STEP*VTA
ISN 0072           YA=TA+273.
ISN 0073           TE=TA+STEP*VTA
ISN 0074           K=1
ISN 0075        82 YE=TE+273.
ISN 0076           CEA=(3.25+0.0085*((TE-TA)/4 /RE))*AE/AR
ISN 0077           FEAA=(0.00425/2./RE)*AE/AR
ISN 0078           FONE=CDC+CDC+EEA*(YE**4-YA**4)+CEA*(TE-TA)-EAS*(YA**4-
          /(YB+DELTA)**4)-CAB*(TA-TB)
ISN 0079           FONED=4.*EEA*YE**3+CEA+(TE-TA)*PEAA
ISN 0080           TENEW=TE-FONE/FONED
ISN 0081           IF (ABS(TENEW-TE)-EPS) 80,80,81
ISN 0082        81 TE=TENEW
ISN 0083           K=K+1
ISN 0084           IF (K-50) 87,87,23
ISN 0085        87 GO TO 82
ISN 0086        80 IF (TENEW-TA) 83,83,84
ISN 0087        83 J=J+1
ISN 0088           GO TO 23
ISN 0089        84 TE=TENEW
ISN 0090           YE=TE+273.
ISN 0091           YX=YE**4-(QBE+QDE-EEA*(YE**4-YA**4)-CEA*(TE-TA))/ERE
ISN 0092           IF (YX) 41,41,44
ISN 0093        41 J=J+1
ISN 0094           GO TO 23
ISN 0095        44 YR=YX**0.25
ISN 0096           TR=YR-273.
ISN 0097           TO=TI+(QBR+QDR+EPE*(YE**4-YR**4))/COEF
ISN 0098           TONEW=(2.*TR+(CCEQ-1.)*TI)/(CCEQ+1.)
ISN 0099           IF (TO-TONEW) 73,73,40
ISN 0100        73 WRITE (6,72) TA,TE,TR,TO,IT
ISN 0101        72 FORMAT (4E12.5,I5///)
ISN 0102           GO TO 27
ISN 0103        40 J=J+1
ISN 0104           GO TO 23
ISN 0105        27 HA(IT)=TA
ISN 0106           HE(IT)=TE
ISN 0107           HR(IT)=TR
ISN 0108           TI=TO
ISN 0109        24 CONTINUE
ISN 0110           NASUM=0.
```

```
      HESUM=0.
      WRSUM=0.
      DO 28 IT=1,NPASS
      HASUM=HASUM+HA(IT)
      HESUM=HESUM+HE(IT)
      WRSUM=WRSUM+WR(IT)
   28 CONTINUE
      TA=HASUM/PASS
      YA=TA+273.
      TE=HESUM/PASS
      YE=TE+273.
      TR=WRSUM/PASS
      YR=TR+273.
      WRITE (6,29) TA,TE,TR,TO
   29 FORMAT (4E12.5///)
      TI=TIN
      WLEN=WLEN*PASS
      AA=AAO*PASS
      AE=AEO*PASS
      AR=ARO*PASS
      CONR=AA/AR
      CEA=(3.25+0.0085*((TE-TA)/4./RE))*AE/AR
      UOPD=ERI+AR*(EEI-1.)/AE
      UOP=SIGMA*(YR**2+YE**2)*(YR+YE)*AR/UOPD
      UNPD=EEI+AE*(EAI-1.)/AA
      UHP=(SIGMA*(YE**2+YA**2)*(YE+YA)/UNPD+CEA*AR/AE)*AE
      UTP=(EA*SIGMA*(YA**4-(YB+DELTA)**4)/(TA-TB)+HAB)*AA
      ULP=UOP*UNP*UTP/(UHP*UTP+UOP*UHP+UOP*UTP)
      UL=ULP/AR
      HIN=2.182*TKF/RI
      UO=1./(1./UL+RO/HIN/RI+AR*ALOG(RO/RRI)/(2.*PI*TKG*WLEN))
      FFR=UO/UL
      ULOH=ULP/UHP
      ULOT=ULP/UTP
      AGFR=UL*FFR*AA*TUBES/FLOWR/CP/CONR
      FRC=1./(AGFR/FFR)
      FSR=FRC*(1.-EXP(-AGFR))
      CR=FLOWR*CP
      CF=FLOWF*CPF
      IF (CR-CF) 30,30,31
   30 CMIN=CR
      CMAX=CF
      GO TO 32
   31 CMIN=CF
      CMAX=CR
      GO TO 32
   32 C=CMIN/CMAX
      TUNIT=UA/CMIN
      EXA=-TUNIT*(1.-C)
      EHX=(1.-EXP(EXA))/(1.-C*EXP(EXA))
      FHXR=CR/CMIN/EHX
      FHXC=FSR*UL*AA*TUBES/CR
      FHX=1./(1.+FHXC*(FHXR-1.))
      CQ=TAM*RMIR**PEFN*TEN*ARN*P
      HTL=HBCI+HD/CONR
      QUY=(HTL*CQ*AA-UL*AR*(TR-TB))*TUBES
      QUZ=AR*FFR*(HTL*CQ-CONR-UL*((TI+TO)/2.-TB))*TUBES
      QU1=FSR*HTL*AR*(CQ+CONR-UL*(TI-TB)/HTL)*TUBES
```

```
ISN 0169          ZO=TAM*(1.-TEM)*ULP/UWP
ISN 0170          ZW=(1.-TEM)*(TAM+(1.-TAM)/(1.-TEM))*ULP/UTP
ISN 0171          QU2=AR*FSR*(HTL*(CP*CONR+ZO+ZW)-UL*(TI-TB))*TUBES
ISN 0172          QU3=QU2*FHX
ISN 0173          QUC=FLOWR*CP*(TO-TI)
ISN 0174          DIVD=(HBCI+HD)*AA*TUBES
ISN 0175          EFFY=QUY/DIVD
ISN 0176          EFFZ=QUZ/DIVD
ISN 0177          EFF1=QU1/DIVD
ISN 0178          EFF2=QU2/DIVD
ISN 0179          EFF3=QU3/DIVD
ISN 0180          EFFC=QUC/DIVD
ISN 0181          WRITE (6,33) UOP,UWP,UTP,ULP,UL,UO
ISN 0182       33 FORMAT (6E12.5///)
ISN 0183          WRITE (6,34) FPR,FSR
ISN 0184       34 FORMAT (2E12.5///)
ISN 0185          WRITE (6,35) CMIN,CMAX,TUNIT,EHX,FHX
ISN 0186       35 FORMAT (5E12.5///)
ISN 0187          WRITE (6,36) QUY,QUZ,QU1,QU2,QU3,QUC
ISN 0188       36 FORMAT (6E12.5///)
ISN 0189          WRITE (6,37) EFFY,EFFZ,EFF1,EFF2,EFF3,EFFC
ISN 0190       37 FORMAT (6E12.5///)
ISN 0191          TI=TO
ISN 0192          TIN=TI
ISN 0193       48 CONTINUE
ISN 0194       74 STOP
ISN 0195          END
```

/ MAIN / SIZE OF PROGRAM 001880 HEXADECIMAL BYTES

NAME	TAG	TYPE	ADD.	NAME	TAG	TYPE	ADD.	NAME	TAG	TYPE	ADD.	NAME	TAG	TYPE	ADD.
C	SF	R*4	00020C	J	SF	I*4	000210	K	SF	I*4	000214	P	SF	R*4	000218
AA	SF	R*4	00021C	AE	SF	R*4	000220	AR	SF	R*4	000224	CF	SF	R*4	000228
CP	SF	R*4	00022C	CQ	SF	R*4	000230	CR	SF	R*4	000234	EA	SF	R*4	000238
EE	SF	R*4	00023C	ER	SF	R*4	000240	HD	SF	R*4	000244	HW	SF	R*4	000248
IT	SF	I*4	00024C	PI	SF	R*4	000250	RE	SF	R*4	000254	RI	SF	R*4	000258
RO	SFA	R*4	00025C	TA	SF	R*4	000260	TB	SF	R*4	000264	TE	SFA	R*4	000268
TI	SF	R*4	00026C	TO	SF	R*4	000270	TR	SF	R*4	000274	UA	SF	R*4	000278
UL	SF	R*4	00027C	UO	SF	R*4	000280	WA	SF	R*4	000440	WE	SF	R*4	000468
WR	SF	R*4	000490	YA	SF	R*4	000284	YB	SF	R*4	000288	YE	SF	R*4	00028C
YR	SF	R*4	000290	YX	SF	R*4	000294	ZO	SF	R*4	000298	ZW	SF	R*4	00029C
AAI	SF	R*4	0002A0	AAN	SF	R*4	0002A4	AAO	SF	R*4	0002A8	AEJ	SF	R*4	0002AC
AEM	SF	R*4	0002B0	AEO	SF	R*4	0002B4	ARK	SF	R*4	0002B8	ARM	SF	R*4	0002BC
ARO	SF	R*4	0002C0	CAB	SF	R*4	0002C4	CEA	SF	R*4	0002C8	CPF	SF	R*4	0002CC
EAI	SF	R*4	0002D0	EAS	SF	R*4	0002D4	EEA	SF	R*4	0002D8	EEI	SF	R*4	0002DC
EHX	SF	R*4	0002E0	EFS	SF	R*4	0002E4	ERE	SF	R*4	0002E8	ERI	SF	R*4	0002EC
EXA	SFA	R*4	0002F0	EXP	F XF	R*4	000000	FAC	SF	R*4	0002F4	FHX	SF	R*4	0002F8
FPR	SF	R*4	0002FC	FRC	SF	R*4	000300	FSR	SF	R*4	000304	GAP	SF	R*4	000308
HAB	SF	R*4	00030C	HIN	SF	R*4	000310	HTL	SF	R*4	000314	HIT	SF	I*4	000318
QBC	SF	R*4	00031C	QBE	SF	R*4	000320	QBR	SF	R*4	000324	QDC	SF	R*4	000328
QDE	SF	R*4	00032C	QDR	SF	R*4	000330	QUC	SF	R*4	000334	QUY	SF	R*4	000338
QUZ	SF	R*4	00033C	QU1	SF	R*4	000340	QU2	SF	R*4	000344	QU3	SF	R*4	000348
RAM	SF	R*4	00034C	REN	SF	R*4	000350	RRI	SFA	R*4	000354	RRM	SF	R*4	000358
TAI	SF	R*4	00035C	TAN	SF	R*4	000360	TEJ	SF	R*4	000364	TEM	SF	R*4	000368
TIN	SF	R*4	00036C	TKF	SF	R*4	000370	TKG	SF	R*4	000374	ULP	SF	R*4	000378
UOP	SF	R*4	00037C	UTP	SF	R*4	000380	UWP	SF	R*4	000384	VTA	SF	R*4	000388
AGFR	SFA	R*4	00038C	ALOG	F XF	R*4	000000	AROL	SF	R*4	000390	CMAX	SF	R*4	000394

APPENDIX B. A COMPUTER PROGRAM TO ANALYZE THERMAL PROCESSES IN A SERIES OF CPC COLLECTORS FITTED WITH HEAT PIPES

The computer program given in this appendix is designed to analyze the thermal processes in a CPC collector fitted with a heat pipe receiver. A single run of the program yields data for ten collectors in series. Line number 66 can be changed if more collectors are needed. Definitions for input variables are given as follows.

RC = r_a

RO = $r_{p,o}$

RE = r_e

HW = w

WLEN = L

GAP = Clearance + $(r_e - r_{p,o})$

REFN = $\bar{n}$

TUBES = No. of troughs in parallel

EVOC = L_e/L_c

HBCJ = $H_b(i)$

HD = H_d

TB = T_b

TI = T_i

FLOWR = $\dot{m}_b$

WIND = V

ER = ε_r

EE = ε_e

EA = ε_a

CP = c_{p_b}

TKF = k_f

ARK = $\alpha_r(k)$

ARM = $\bar{\alpha}_r$

RRM = $\bar{\rho}_r$

AEJ = $\alpha_e(j)$

AEM = $\bar{\alpha}_e$

REM = $\bar{\rho}_e$

TEJ = $\tau_e(j)$

TEM = $\bar{\tau}_e$

AAI = $\alpha_a(i)$

AAM = $\bar{\alpha}_a$

RAM = $\bar{\rho}_a$

TAI = $\tau_a(i)$

TAM = $\bar{\tau}_a$

RMIR = ρ_m

EPS = Convergence criterion for iteration

PASS = No. of troughs in series

UHP = U_p

Definitions for output variables are given as follows:

TA = T_a or $\bar{T}_a$

TE = T_e or $\bar{T}_e$

TR = T_r or $\bar{T}_r$

TO = T_o

UOP = $U_{r/e}\ A_r$

UWP = $U_{e/a}\ A_e$

UTP = $U_{a/b}\ A_a$

ULP = $U_L\ A_r$

UL = U_L

UO = U_o

FPR = F'

FSR = F_R

QUY = Q_u, Equation (28)

QUZ = Q_u, Equation (29)

QU1 = Q_u, Equation (32)

QU2 = Q_u, Equation (34)

QUC = $\dot{m}_b\ c_{p_b}\ (T_o - T_i)_b$

EFFY = η, Equation (39)

EFFZ = η, Equation (40)

EFF1 = η, Equation (41)

EFF2 = η, Equation (42)

EFFC = η, Equation (45)

The computer program is given on the next page. A set of data output is given following the computer program. This is the group of data used in making the system analysis given in Section III, 2.

```
LEVEL 2.2  (SEPT 76)                 OS/360  FORTRAN H EXTENDED           DATE 79.240/13.53.03        PAGE   1

REQUESTED OPTIONS: NOTERM,

OPTIONS IN EFFECT: NAME(MAIN) NOOPTIMIZE LINECOUNT(60) SIZE(MAX) AUTODBL(NONE)
                   SOURCE EBCDIC NOLIST NODECK OBJECT MAP NOFORMAT GOSTMT NOXREF NOALC NOANSF NOTERM FLAG(I)

                C      THIS PROGRAM SIMULATES THERMAL PROCESSES IN A CPC
   ISN 0002            DIMENSION HA(10),HE(10),HR(10)
   ISN 0003            READ (5,1) RC,RO,RE,HH,HLEN,GAP,REFN,TUBES,EVOC
   ISN 0004          1 FORMAT (9F8.4)
   ISN 0005            READ (5,2) HDCI,HD,TB,TI,FLOWR,WIND
   ISN 0006          2 FORMAT (6F8.4)
   ISN 0007            READ (5,3) ER,EE,EA,CP,TKF
   ISN 0008          3 FORMAT (5F8.4)
   ISN 0009            READ (5,4) ARK,ARM,RRM,AEJ,AEM,PEM,TEJ,TEM
   ISN 0010          4 FORMAT (8F8.4)
   ISN 0011            READ (5,5) AAI,AAM,PAM,TAI,TAM,RNIR
   ISN 0012          5 FORMAT (6F8.4)
   ISN 0013            READ (5,11) EPS,PASS,UHP
   ISN 0014         11 FORMAT (3F10.5)
   ISN 0015            WRITE (6,17)
   ISN 0016         17 FORMAT (12H INPUT DATA:///)
   ISN 0017            WRITE (6,6) RC,RO,RE,HH,HLEN,GAP,REFN,TUBES,EVOC
   ISN 0018          6 FORMAT (9F10.4///)
   ISN 0019            WRITE (6,7) HDCI,HD,TB,TI,FLOWR,WIND
   ISN 0020          7 FORMAT (6F10.4///)
   ISN 0021            WRITE (6,8) ER,EE,EA,CP,TKF
   ISN 0022          8 FORMAT (5F10.4///)
   ISN 0023            WRITE (6,9) ARK,ARM,RRM,AEJ,AEM,PEM,TEJ,TEM
   ISN 0024          9 FORMAT (8F10.4///)
   ISN 0025            WRITE (6,10) AAI,AAM,PAM,TAI,TAM,RNIR
   ISN 0026         10 FORMAT (6F10.4///)
   ISN 0027            WRITE (6,16) EPS,PASS,UHP
   ISN 0028         16 FORMAT (3F10.5///)
   ISN 0029            NPASS=PASS
   ISN 0030            TIN=TI
   ISN 0031            PI=3.14159
   ISN 0032            SIGMA=5.668E-8
   ISN 0033            DELTA=-6.
   ISN 0034            YB=TB+273.
   ISN 0035            AR=2.*PI*RO*HLEN
   ISN 0036            AE=2.*PI*RE*HLEN
   ISN 0037            AA=2.*HH*HLEN
   ISN 0038            ARO=AR
   ISN 0039            AEO=AE
   ISN 0040            AAO=AA
   ISN 0041            AROL=AR/HLEN
   ISN 0042            P=1.-(GAP/AROL)
   ISN 0043            RNIRE=RNIR**REFN
   ISN 0044            RNIR=HDCI*TAI*RNIRE
   ISN 0045            ERI=1./ER
   ISN 0046            EEI=1./EE
   ISN 0047            EAI=1./EA
   ISN 0048            COEF=FLOWR*CP/TUBES/AR
   ISN 0049            FAC=HLEN/AR
   ISN 0050            ARC=AR/EVOC
   ISN 0051            ACC=PI*RO**2
   ISN 0052            HCON=2.0315*TKF/(RC-RO)
   ISN 0053            RHRF=1./(UHP*ACC)+1./(HCON*ARC)
```

```
ISN 0054          COEG=1./2./RHPF/AR
ISN 0055          COEQ=COEF/COEG
ISN 0056          QBR=HBTR*TEJ*P*(ARK+ARM*RRM*REM*AR/AE)*AA/AR
ISN 0057          QBC=HBCI*(AAI+AAN*TAI*REN*RMIRE**2)*AA/AR
ISN 0058          QBE=HBTR*(AEJ+AEN*REN*PAN*RMIRE**2*AE/AA+AEM*RRM*TEJ)*AA/AR
ISN 0059          QDR=HD*TAN*TEN*ARN*RMIRE*P*(1.+RRN*REM*AR/AE)
ISN 0060          QDC=HD*AAN*(1.+TAN*REN*RMIRE**2)*AA/AR
ISN 0061          QDE=HD*TAN*RMIRE*AEN*(1.+REN*RAN*RMIRE**2*AE/AA+RRM*TEM)
ISN 0062          ERE=SIGMA/(ERI+AR*(EEI-1.)/AE)
ISN 0063          EEA=(AE/AR)*SIGMA/(EEI+AE*(EAI-1.)/AA)
ISN 0064          EAS=EA*SIGMA*AA/AR
ISN 0065          HAB=5.7+3.8*WIND
ISN 0066          CAB=HAB*AA/AR
ISN 0067          STEP=0.01
ISN 0068          DO 48 MIT=1,10
ISN 0069          WRITE (6,21) MIT
ISN 0070       21 FORMAT (1H1,30H OUTPUT DATA FOR COLLECTOR NO.I2,1H:///)
ISN 0071       22 DO 24 IT=1,NPASS
ISN 0072          J=1
ISN 0073       23 VTA=J
ISN 0074          IF (J-600) 25,25,74
ISN 0075       25 TA=TB+STEP*VTA
ISN 0076          YA=TA+273.
ISN 0077          TE=TA+STEP*VTA
ISN 0078          K=1
ISN 0079       82 YE=TE+273.
ISN 0080          CEA=(3.25+0.0085*((TE-TA)/4./RE))*AE/AR
ISN 0081          PEAA=(0.00425/2./RE)*AE/AR
ISN 0082          FONE=QDC+CDC+EEA*(YE**4-YA**4)+CEA*(TE-TA)-EAS*(YA**4-
                 /(YB+DELTA)**4)-CAB*(TA-TB)
ISN 0083          FONED=4.*EEA*YE**3+CEA+(TE-TA)*PEAA
ISN 0084          TENEW=TE-FONE/FONED
ISN 0085          IF (ABS(TENEW-TE)-EPS) 80,80,81
ISN 0086       81 TE=TENEW
ISN 0087          K=K+1
ISN 0088          IF (K-50) 87,87,23
ISN 0089       87 GO TO 82
ISN 0090       80 IF (TENEW-TA) 83,83,84
ISN 0091       83 J=J+1
ISN 0092          GO TO 23
ISN 0093       84 TE=TENEW
ISN 0094          YE=TE+273.
ISN 0095          YX=YE**4-(QBE+QDE-EEA*(YE**4-YA**4)-CEA*(TE-TA))/ERE
ISN 0096          IF (YX) 41,41,44
ISN 0097       41 J=J+1
ISN 0098          GO TO 2
ISN 0099       44 YR=YX**0.25
ISN 0100          TR=YR-273.
ISN 0101          TO=TI+(QBR+QDR+EPE*(YE**4-YR**4))/COEF
ISN 0102          TONEW=(2.*TR+(COEQ-1.)*TI)/(COEQ+1.)
ISN 0103          IF (TO-TONEW) 73,73,40
ISN 0104       73 WRITE (6,72) TA,TE,TR,TO,IT
ISN 0105       72 FORMAT (4E12.5,I5///)
ISN 0106          GO TO 27
ISN 0107       40 J=J+1
ISN 0108          GO TO 23
ISN 0109       27 WA(IT)=TA
ISN 0110          WE(IT)=TE
```

```
      WR(IT)=TR
      TI=TO
   24 CONTINUE
      WASUM=0.
      WESUM=0.
      WRSUM=0.
      DO 28 IT=1,NPASS
      WASUM=WASUM+WA(IT)
      WESUM=WESUM+WE(IT)
      WRSUM=WRSUM+WR(IT)
   28 CONTINUE
      TA=WASUM/PASS
      YA=TA+273.
      TE=WESUM/PASS
      YE=TE+273.
      TR=WRSUM/PASS
      YR=TR+273.
      WRITE (6,29) TA,TE,TR,TO
   29 FORMAT (4E12.5///)
      TI=TIN
      WLEN=WLEN*PASS
      AA=AAO*PASS
      AE=AEO*PASS
      AR=ARO*PASS
      CONR=AA/AR
      CEA=(3.25+0.0085*((TE-TA)/4./RE))*AE/AR
      UOPD=ERI+AR*(EEI-1.)/AE
      UOP=SIGMA*(YR**2+YE**2)*(YR+YE)*AR/UOPD
      UWPD=EEI+AE*(EAI-1.)/AA
      UWP=(SIGMA*(YE**2+YA**2)*(YE+YA)/UWPD+CEA*AR/AE)*AE
      UTP=(EA*SIGMA*(YA**4-(TB+DELTA)**4)/(TA-TB)+HAB)*AA
      ULP=UOP*UWP*UTP/(UWP*UTP+UOP*UWP+UOP*UTP)
      UL=ULP/AR
      AZY=ACC/ARC
      UO=1./(1./UL+ARO/UHP/ACC+EVOC/HCON)
      FFR=UO/UL
      ULOW=ULP/UWP
      ULOT=ULP/UTP
      AGFR=UL*FFR*AA/FLOWR/CP/CONR
      FRC=1./(AGFR/FFR)
      FSR=FRC*(1.-EXP(-AGFR))
      CQ=TAM*RMIR**PEFN*TEM*APM*P
      HTL=HDCI+HD/CONR
      QUY=HTL*CQ*AA-UL*AR*(TR-TB)
      QUZ=AR*FFR*(HTL*CQ*CONR-UL*((TI+TO)/2.-TB))
      QU1=FSR*HTL*AR*(CQ*CONR-UL*(TI-TB)/HTL)
      ZO=TAM*(1.-TEM)*ULP/UWP
      ZN=(1.-TEM)*(TAM+(1.-TAM)/(1.-TEM))*ULP/UTP
      QU2=AR*FSR*(HTL*(CQ*CONR+ZO+ZN)-UL*(TI-TB))
      QUC=FLOWR*CP*(TO-TI)
      DIVD=(HDCI+HD)*AA
      EFFY=QUY/DIVD
      EFFZ=QUZ/DIVD
      EFF1=QU1/DIVD
      EFF2=QU2/DIVD
      EFFC=QUC/DIVD
      WRITE (6,33) UOP,UWP,UTP,ULP,UL,UO
   33 FORMAT (6E12.5///)
```

```
ISN 0169           WRITE (6,34) FPR,FSR
ISN 0170        34 FORMAT (2E12.5///)
ISN 0171           WRITE (6,36) QUY,QUZ,QU1,QU2,QUC
ISN 0172        36 FORMAT (5E12.5///)
ISN 0173           WRITE (6,37) EFFY,EFFZ,EFF1,EFF2,EFFC
ISN 0174        37 FORMAT (5E12.5///)
ISN 0175           TI=TO
ISN 0176           TIN=TI
ISN 0177        48 CONTINUE
ISN 0178        74 STOP
ISN 0179           END
```

/ MAIN / SIZE OF PROGRAM 001658 HEXADECIMAL BYTES

NAME	TAG	TYPE	ADD.	NAME	TAG	TYPE	ADD.	NAME	TAG	TYPE	ADD.	NAME	TAG	TYPE	ADD.
J	SF	I*4	0001EC	K	SF	I*4	0001F0	P	SF	R*4	0001F4	AA	SF	R*4	0001F8
AE	SF	R*4	0001FC	AR	SF	R*4	000200	CP	SF	R*4	000204	CQ	SF	R*4	000208
EA	SF	R*4	00020C	EE	SF	R*4	000210	ER	SF	R*4	000214	HD	SF	R*4	000218
HH	SF	R*4	00021C	IT	SF	I*4	000220	PI	SF	R*4	000224	RC	SF	R*4	000228
RE	SF	R*4	00022C	RO	SF	R*4	000230	TA	SF	R*4	000234	TB	SF	R*4	000238
TE	SFA	R*4	00023C	TI	SF	R*4	000240	TO	SF	R*4	000244	TR	SF	R*4	000248
UL	SF	R*4	00024C	UD	SF	R*4	000250	HA	SF	R*4	0003F0	HE	SF	R*4	000418
WR	SF	R*4	000440	YA	SF	R*4	000254	YB	SF	R*4	000258	YE	SF	R*4	00025C
YR	SF	R*4	000260	YX	SF	R*4	000264	ZO	SF	R*4	000268	ZH	SF	R*4	00026C
AAI	SF	R*4	000270	AAM	SF	R*4	000274	AAO	SF	R*4	000278	ACC	SF	R*4	00027C
AEJ	SF	R*4	000280	AEN	SF	R*4	000284	AEO	SF	R*4	000288	ARC	SF	R*4	00028C
ARK	SF	R*4	000290	ARM	SF	R*4	000294	ARO	SF	R*4	000298	AZY	S	R*4	00029C
CAB	SF	R*4	0002A0	CEA	SF	R*4	0002A4	EAI	SF	R*4	0002A8	EAS	SF	R*4	0002AC
EEA	SF	R*4	0002B0	EEI	SF	R*4	0002B4	EPS	SF	R*4	0002B8	ERE	SF	R*4	0002BC
ERI	SF	R*4	0002C0	EXP	F XF	R*4	000000	FAC	S	R*4	0002C4	FPR	SF	R*4	0002C8
FRC	SF	R*4	0002CC	FSR	SF	R*4	0002D0	GAP	SF	R*4	0002D4	HAB	SF	R*4	0002D8
HTL	SF	R*4	0002DC	HIT	SF	I*4	0002E0	QBC	SF	R*4	0002E4	QBE	SF	R*4	0002E8
QBR	SF	R*4	0002EC	QDC	SF	R*4	0002F0	QDE	SF	R*4	0002F4	QDR	SF	R*4	0002F8
QUC	SF	R*4	0002FC	QUY	SF	R*4	000300	QUZ	SF	R*4	000304	QU1	SF	R*4	000308
QU2	SF	R*4	00030C	RAM	SF	R*4	000310	REM	SF	R*4	000314	RRM	SF	R*4	000318
TAI	SF	R*4	00031C	TAM	SF	R*4	000320	TEJ	SF	R*4	000324	TEM	SF	R*4	000328
TIN	SF	R*4	00032C	TKF	SF	R*4	000330	UHP	SF	R*4	000334	ULP	SF	R*4	000338
UCP	SF	R*4	00033C	UTP	SF	R*4	000340	UNP	SF	R*4	000344	VTA	SF	R*4	000348
AGFR	SFA	R*4	00034C	AROL	SF	R*4	000350	COEF	SF	R*4	000354	COEG	SF	R*4	000358
COEQ	SF	R*4	00035C	CONR	SF	R*4	000360	DIVD	SF	R*4	000364	EFFC	SF	R*4	000368
EFFY	SF	R*4	00036C	EFFZ	SF	R*4	000370	EFF1	SF	R*4	000374	EFF2	SF	R*4	000378
EVOC	SF	R*4	00037C	FCNE	SF	R*4	000380	HBCI	SF	R*4	000384	HBTR	SF	R*4	000388
HCON	SF	R*4	00038C	PASS	SF	R*4	000390	PEAA	SF	R*4	000394	REFN	SF	R*4	000398
RHPF	SF	R*4	00039C	RHIR	SF	R*4	0003A0	STEP	SF	R*4	0003A4	ULOT	S	R*4	0003A8
ULCH	S	R*4	0003AC	UPFD	SF	R*4	0003B0	UNFD	SF	R*4	0003B4	WIND	SF	R*4	0003B8
WLEN	SF	R*4	0003BC	DELTA	SF	R*4	0003C0	FLOWR	SF	R*4	0003C4	FONED	SF	R*4	0003C8
NPASS	SF	I*4	0003CC	RHIRE	SF	R*4	0003D0	SIGMA	SF	R*4	0003D4	TENEH	SFA	R*4	0003D8
TONEH	S	R*4	0003DC	TUBES	SF	R*4	0003E0	WASUM	SF	R*4	0003E4	WESUM	SF	R*4	0003E8
WRSUM	SF	R*4	0003EC	FRXPR#	XF	R*4	000000	IBCOM#	F XF	I*4	000000				

SOURCE STATEMENT LABELS

LABEL	ISN	ADDR	LABEL	ISN	ADDR	LABEL	ISN	ADDR	LABEL	ISN	ADDR
22	71	000C2C NR	23	73	000C3C	25	75	000C62	82	79	000C92
81	86	000DCC	87	89	000DEA	80	90	000DF0	83	91	000DFE

INPUT DATA:

```
  0.0127    0.0095    0.0174    0.1128    1.2192    0.0129    0.6000    1.0000    8.0000

966.0000  100.0000   20.0000  137.3900    0.0170    5.0000

  0.0500    0.8500    0.8500 4170.0000    0.6500

  0.8500    0.8500    0.1500    0.0500    0.0500    0.0500    0.9000    0.9000

  0.0500    0.0500    0.0500    0.9000    0.9000    0.8500

 0.01000   5.000009180.00000
```

```
 OUTPUT DATA FOR COLLECTOR NO. 1:

0.23740E+02 0.39725E+02 0.21011E+03 0.13915E+03     1

0.23760E+02 0.39840E+02 0.21189E+03 0.14091E+03     2

0.23780E+02 0.39956E+02 0.21366E+03 0.14267E+03     3

0.23800E+02 0.40071E+02 0.21540E+03 0.14443E+03     4

0.23820E+02 0.40186E+02 0.21713E+03 0.14618E+03     5

0.23780E+02 0.39956E+02 0.21364E+03 0.14618E+03

0.27542E+00 0.68699E+01 0.51015E+02 0.26344E+00 0.72208E+00 0.70098E+00

0.97078E+00 0.96902E+00

0.61715E+03 0.61749E+03 0.61749E+03 0.61905E+03 0.62306E+03

0.42106E+00 0.42129E+00 0.42129E+00 0.42235E+00 0.42509E+00
```

OUTPUT DATA FOR COLLECTOR NO. 2:

```
0.23840E+02 0.40301E+02 0.21834E+03 0.14793E+03    1

0.23850E+02 0.40358E+02 0.21969E+03 0.14968E+03    2

0.23870E+02 0.40473E+02 0.22137E+03 0.15143E+03    3

0.23890E+02 0.40587E+02 0.22304E+03 0.15317E+03    4

0.23910E+02 0.40701E+02 0.22468E+03 0.15492E+03    5

0.23872E+02 0.40484E+02 0.22152E+03 0.15492E+03

0.28502E+00 0.69159E+01 0.59775E+02 0.27227E+00 0.74631E+00 0.72379E+00

0.96983E+00 0.96802E+00

0.61329E+03 0.61353E+03 0.61353E+03 0.61513E+03 0.61930E+03

0.41842E+00 0.41859E+00 0.41859E+00 0.41968E+00 0.42252E+00
```

OUTPUT DATA FOR COLLECTOR NO. 3:

```
0.23930E+02 0.40815E+02 0.22632E+03 0.15666E+03     1

0.23950E+02 0.40929E+02 0.22793E+03 0.15839E+03     2

0.23980E+02 0.41099E+02 0.23033E+03 0.16013E+03     3

0.24000E+02 0.41212E+02 0.23191E+03 0.16186E+03     4

0.24020E+02 0.41324E+02 0.23347E+03 0.16359E+03     5

0.23976E+02 0.41076E+02 0.22999E+03 0.16359E+03

0.29504E+00 0.69674E+01 0.50516E+02 0.28202E+00 0.77302E+00 0.74889E+00

0.96878E+00 0.96692E+00

0.60894E+03 0.60925E+03 0.60926E+03 0.61091E+03 0.61504E+03

0.41545E+00 0.41567E+00 0.41568E+00 0.41680E+00 0.41962E+03
```

OUTPUT DATA FOR COLLECTOR NO. 4:

```
0.24040E+02 0.41437E+02 0.23502E+03 0.16532E+03    1

0.24060E+02 0.41550E+02 0.23656E+03 0.16704E+03    2

0.24080E+02 0.41662E+02 0.23808E+03 0.16877E+03    3

0.24100E+02 0.41774E+02 0.23959E+03 0.17049E+03    4

0.24120E+02 0.41886E+02 0.24109E+03 0.17221E+03    5

0.24080E+02 0.41662E+02 0.23807E+03 0.17221E+03

0.30604E+00 0.70183E+01 0.50271E+02 0.29155E+00 0.799[illegible]4E+00 0.77338E+00

0.96776E+00 0.96584E+00

0.60458E+03 0.60489E+03 0.60490E+03 0.60660E+03 0.61079E+03

0.41248E+00 0.41269E+00 0.41270E+00 0.41386E+00 0.41672E+00
```

OUTPUT DATA FOR COLLECTOR NO. 5:

0.24150E+02 0.42053E+02 0.24330E+03 0.17392E+03 1

0.24170E+02 0.42165E+02 0.24477E+03 0.17564E+03 2

0.24190E+02 0.42276E+02 0.24622E+03 0.17735E+03 3

0.24210E+02 0.42387E+02 0.24766E+03 0.17905E+03 4

0.24230E+02 0.42498E+02 0.24909E+03 0.18076E+03 5

0.24190E+02 0.42276E+02 0.24621E+03 0.18076E+03

0.31682E+00 0.70717E+01 0.50026E+02 0.30141E+00 0.82616E+00 0.79865E+00

0.96671E+00 0.96473E+00

0.59998E+03 0.60032E+03 0.60033E+03 0.60207E+03 0.60629E+03

0.40934E+00 0.40958E+00 0.40958E+00 0.41077E+00 0.4136[illegible]E+00

OUTPUT DATA FOR COLLECTOR NO. 6:

```
0.24260E+02 0.42663E+02 0.25120E+03 0.18246E+03     1

0.24280E+02 0.42773E+02 0.25260E+03 0.18416E+03     2

0.24300E+02 0.42833E+02 0.25399E+03 0.18586E+03     3

0.24330E+02 0.43048E+02 0.25605E+03 0.18755E+03     4

0.24350E+02 0.43158E+02 0.25741E+03 0.18925E+03     5

0.24304E+02 0.42905E+02 0.25425E+03 0.18925E+03

0.32776E+00 0.71264E+01 0.49785E+02 0.31139E+00 0.85352E+00 0.82419E+00

0.96564E+00 0.96360E+00

0.59522E+03 0.59559E+03 0.59560E+03 0.59739E+03 0.60162E+03

0.40609E+00 0.40635E+00 0.40636E+00 0.40758E+00 0.41047E+00
```

OUTPUT DATA FOR COLLECTOR NO. 7:

0.24370E+02 0.43267E+02 0.25876E+03 0.19094E+03 1

0.24400E+02 0.43431E+02 0.26077E+03 0.19262E+03 2

0.24420E+02 0.43540E+02 0.26210E+03 0.19431E+03 3

0.24440E+02 0.43649E+02 0.26341E+03 0.19599E+03 4

0.24470E+02 0.43812E+02 0.265[illegible]E+03 0.19767E+03 5

0.24420E+02 0.43540E+02 0.26208E+03 0.19767E+03

0.33369E+00 0.71814E+01 0.49552E+02 0.32134E+00 0.83080E+00 0.84960E+00

0.96458E+00 0.96243E+00

0.59037E+03 0.59073E+03 0.59075E+03 0.59258E+03 0.59083E+03

0.40279E+00 0.40303E+00 0.40304E+00 0.40429E+00 0.40723E+00

OUTPUT DATA FOR COLLECTOR NO. 8:

```
0.24490E+02 0.43920E+02 0.26656E+03 0.19934E+03    1

0.24520E+02 0.44082E+02 0.26858E+03 0.20101E+03    2

0.24540E+02 0.44190E+02 0.26985E+03 0.20268E+03    3

0.24560E+02 0.44298E+02 0.27111E+03 0.20435E+03    4

0.24590E+02 0.44459E+02 0.27299E+03 0.20602E+03    5

0.24540E+02 0.44190E+02 0.26984E+03 0.20602E+03

0.34980E+00 0.72378E+01 0.49324E+02 0.33143E+00 0.90845E+00 0.87530E+00

0.96351E+00 0.96134E+00

0.58536E+03 0.58571E+03 0.58572E+03 0.58760E+03 0.59196E+03

0.39937E+00 0.39961E+00 0.39961E+00 0.40090E+00 0.40387E+00
```

OUTPUT DATA FOR COLLECTOR NO. 9:

0.24610E+02 0.44566E+02 0.27423E+03 0.20768E+03 1

0.24640E+02 0.44727E+02 0.27607E+03 0.20934E+03 2

0.24660E+02 0.44833E+02 0.27729E+03 0.21099E+03 3

0.24690E+02 0.44993E+[illegible] 0.27910E+03 0.21265E+03 4

0.24720E+02 0.45153E+02 0.28090E+03 0.21430E+03 5

0.24664E+02 0.44854E+02 0.27752E+03 0.21430E+03

0.36107E+00 0.72954E+01 0.49102E+02 0.34165E+00 0.93646E+00 0.90128E+00

0.96243E+00 0.96020E+00

0.58018E+03 0.58053E+03 0.58054E+03 0.58247E+03 0.58688E+03

0.39583E+00 0.39607E+00 0.39608E+00 0.39739E+00 0.40041E+00

OUTPUT DATA FOR COLLECTOR NO. 10:

```
0.24740E+02 0.45259E+02 0.28209E+03 0.21594E+03    1

0.24770E+02 0.45418E+02 0.28385E+03 0.21759E+03    2

0.24790E+02 0.45523E+02 0.28502E+03 0.21923E+03    3

0.24820E+02 0.45682E+02 0.28676E+03 0.22086E+03    4

0.24850E+02 0.45840E+02 0.28848E+03 0.22250E+03    5

0.24794E+02 0.45544E+02 0.28524E+03 0.22250E+03

0.37269E+00 0.73551E+01 0.48881E+02 0.35216E+00 0.96527E+00 0.92793E+00

0.96132E+00 0.95903E+00

0.57475E+03 0.57515E+03 0.57516E+03 0.57714E+03 0.58156E+03

0.39213E+00 0.39240E+00 0.39241E+00 0.39376E+00 0.39678E+00
```